FCTUC FACULDADE DE CIÊNCIAS
E TECNOLOGIA
UNIVERSIDADE DE COIMBRA

DEPARTAMENTO DE
ENGENHARIA MECÂNICA

The effect of V content on the structure, mechanical properties, and tribological behaviour of Ti-Si-V-N films deposited by HiPIMS in deep oscillation magnetron sputtering (DOMS) mode

Submitted in Partial Fulfilment of the Requirements for the Degree of Master in Materials Engineering

Author

Melkamu Awoke Mekicha

Advisors

Professor **Albano Cavaleiro**
Doctor **Filipe Daniel Fernandes**

Jury

President	**Bruno Trindade** **Professor at University of Coimbra**
Vowel	**Ana Manaia** **Researcher at Instituto Pedro Nunes**
Advisor	**Filipe Daniel Fernandes** **Postdoctoral researcher at CEMUC, University of Coimbra**

In the framework of Joint European Master in tribology of Surfaces and Interfaces

tribos joint european master in tribology of surfaces and interfaces
Ljubljana • Leeds • Coimbra • Luleå

Coimbra, July, 2015

Acknowledgement

First and foremost, I offer my sincerest gratitude to my advisor Dr. FILIPE DANIEL FERNANDES, who has supported me throughout my thesis with his patience and knowledge whilst allowing me to explore on my own, and at the same time the guidance to recover when my steps faltered. You have been a tremendous mentor for me, one simply could not wish for a better or friendlier advisor. I would also like to take this opportunity to thank professor Albano Cavaleiro for giving me the opportunity to visit different scientific research centres.

My special thanks are to the TRIBOS consortium, which at the first place gave me the opportunity to join this prestigious program. My thanks are also to all first batch TRIBOS students for the wonderful times we had together and invaluable life lessons I learned during the last two years. I would also want to thank all researchers in CEMUC, especially Fabio Ferreira, for the friendly and cheerful time I had. My sincere thanks are to my friends and all the people who helped me, in one way or another, to complete this thesis. Last but not least, I am grateful to my family for supporting me throughout my life.

Abstract

Self-lubricant coatings have been developed by combining the intrinsic properties of some binary and ternary coating systems, that are resistant to oxidation, with some elements that diffuse to the surface as a metal and/or forming oxides and fluorides to get the lubricious properties. Magnéli oxide phases, which possess thermal stability and easy shear planes, have been proposed to achieve lubrication at elevated temperatures. Additions of V to dissimilar coating systems showed to successfully improve their tribological behaviour at high temperatures due to the formation of lubricious V_2O_5. However, such improvement do not last long due to the fast diffusion of V to the surface. Thus, the challenge now is the control of lubricious metal diffusion to the surface, a criterion required to achieve long term lubrication.

The aim of this thesis is to study the effect of V addition on the structure, mechanical properties and tribological behaviour of Ti-Si-V-N films deposited by high power impulse magnetron sputtering (HiPIMS) in deep oscillation mode (DOMS). TiSiN system has been selected because of its high oxidation resistance and excellent mechanical properties. Further, if deposited in nanocomposite structure with a nanocrystalline TiN grain embedded by amorphous SiN phase, the later phase can act as a diffusion barrier and allow control out diffusion of V. DOMS was selected as deposition process as it has been reported to easily obtain and tailor the nanocomposite structure of TiSiN films. The crystal structure of films was analyzed by X-ray diffraction (XRD). The microstructure of the films was characterized by scanning electron microscopy (SEM) while their mechanical properties were measured by nanoindentation and scratch tests. Further, the tribological behaviour of coatings was evaluated by reciprocating sliding equipment. The wear mechanism present on the wear track of coatings was investigated by SEM and the wear debris analysed by energy dispersive x-ray spectroscopy (SEM-EDS) and Raman spectroscopy.

A total of twelve depositions of dissimilar TiSi(V)N coatings were deposited using HiPIMS process in DOMS mode with 7 and 12 at.% Si content. For each silicon content, three depositions with different vanadium content (0, 6, and 11 at.% V) were made. All the above depositions were done twice using low peak power (28 kW) and high peak power (68 kW for films with 7 at.% Si and 109 kW for films with 12 at.% Si). All films made at low peak powers showed a columnar microstructure and cauliflower surface morphology, while those deposited using high peak power had a compact microstructure and granular surface morphology. V addition and silicon content had little influence on the surface and cross morphology of the coatings. A shift of diffraction peaks to higher angles with V addition suggested the formation of substitutional solid solution in TiN phase. Coatings deposited at high peak power showed higher hardness and higher level of compressive residual stresses as compared to those deposited at low peak powers. Tribological tests indicated that V addition decreased the friction coefficient. In addition, TiSiVN films with 11 at.% V, irrespective of the peak power used and silicon content, showed excellent wear resistance Abrasion wear took place for the dissimilar TiSiN coatings deposited as reference, whereas polishing wear was observed for all V rich films.

key words: DOMS, TISi(V)N films, Structure, mechanical properties, tribology

Resumo

Revestimentos auto-lubrificantes têm sido desenvolvidos através da combinação das propriedades intrínsecas de alguns sistemas de revestimento binários ou ternários, que são resistentes à oxidação, com alguns elementos que se difundem para a superfície sob forma de metal e/ou formando óxidos e fluoretos para obter propriedades lubrificantes. O uso deste tipo de revestimentos, baseados na formação de óxidos com propriedades lubrificantes foram propostos para promover lubrificação a alta temperatura. A adição de vanádio mostrou melhorar as propriedades tribológicas de vários sistemas de revestimentos a alta temperatura devido à formação da fase lubrificante V_2O_5. Contudo, estas melhorias tribológicas mostraram ser de curta duração devido à rápida e total difusão de vanádio para a superfície. Portanto, o desafio para desenvolver revestimentos autolubrificantes que promovam lubrificação contínua durante um longo período de tempo, passa pelo controlo adequado da difusão do metal que promove propriedades lubrificantes, para a superfície.

O objetivo desta tese é estudar o efeito da adição de V na estrutura, propriedades mecânicas e comportamento tribológico de revestimentos Ti-Si-V-N depositados por *high power impulse magnetron sputtering (HiPIMS)* em *deep oscillation mode (DOMS)*, uma variante do HiPIMS em que os impulsos de potência são constituídos por conjuntos de oscilações. Revestimentos do tipo TiSiN foram seleccionados devido à sua excelente resistência à oxidação e propriedades mecânicas. Além disso, quando este sistema de revestimentos for depositado com uma estrutura nanocompósita, isto é, grãos nanocristalinos de TiN embebidos numa matriz amorfa de SiN, a última fase pode atuar como uma barreira de difusão e portanto permitir controlar a difusão de V. O processo de deposição DOMS foi seleccionado para produzir estes filmes, uma vez que foi demonstrado facilmente permitir obter e alterar a estrutura nanocompósita dos revestimentos TISiN. A estrutura cristalina dos revestimentos foi analisada com recurso ao equipamento de difracção de raios-x. A microestrutura foi caraterizada por microscópio de varrimento electrónica (SEM), enquanto que, as suas propriedades mecânicas foram avaliadas por nano-indentação e testes de indentação deslizante. Além disso, as propriedades tribológicas dos revestimentos foram avaliadas por ensaios de desgaste alternativos (reciprocating sliding). Os mecanismos de desgaste presentes nas pistas de desgaste foram identificados por observações SEM e os detritos resultantes do desgaste analisados por SEM e espectroscopia Raman.

Um total de 12 revestimentos foram depositados por HiPIMS em modo DOMS contendo 7 e 12% atómico de Si. Para cada um dos teores de silício, 3 revestimentos com diferentes teores de vanádio (0, 6, and 11 at.% de V) foram produzidos. As deposições acima referidas foram realizadas 2 vezes, usando baixa potência de pico e alta potência de pico (68.17 kW para os revestimentos com 7 at.% de Si e 109.83 kW para os revestimentos com 12 at.% de Si). Todos os revestimentos depositados com baixa potência de pico mostraram possuir uma microestrutura colunar e uma morfologia superficial do tipo couve-flor, enquanto que aqueles depositados com elevada potência de pico mostraram uma microestrutura mais compacta e uma morfologia superficial do tipo granular. A adição de vanádio e silício aos revestimentos mostraram não alterar significativamente a microestrutura e morfologia superficial dos revestimentos. O desvio dos picos de difracção para a direita com o aumento do teor em V nos

revestimentos, sugeriu a formação de solução sólida substitucional. Os revestimentos depositados com alta potência de pico mostraram possuir valores dureza e tensões residuais de compressa mais elevados do que os revestimentos depositados com baixa potência de pico. Os ensaios de desgaste mostraram que a adição de V diminui o coeficiente de atrito dos revestimentos; em alguns casos mais de metade. Além disso, independentemente da potência de pico usada nas deposições e do teor de Si nos revestimentos, aqueles depositados com 11 at.% de V mostraram ser os mais resistentes ao desgaste. Desgaste por Abrasão mostrou ser o mecanismo de desgaste predominante nos diferentes revestimentos de TiSiN depositados como referência, ao passo que, desgaste por polimento mostrou ser o mecanismo de desgaste ativo em todos os revestimentos ricos em V.

Palavras chave: DOMS, TiSi(V)N filmes, Estrutura, Propriedades mecânicas, Tribologia

Table of contents

List of figures

List of tables

List of symbols and acronyms

Symbols

a – amorphous

E – Young's modulus

H – Hardness

Ip – peak current

nc - nanocrystalline

Pp – peak power

Vp – peak voltage

Acronyms

DCMS – direct current magnetron sputtering

DOMS – deep oscillation magnetron sputtering

fcc – face centred cubic

FWHM – full width at half maximum

GIXRD – grazing incidence x-ray diffraction

HIPIMS – high power impulse magnetron sputtering

HPPMS – high power pulsed magnetron sputtering

HV – Vickers hardness

ICDD – International centre for diffraction data

MPPS – modulated pulsed power magnetron sputtering

Chapter I

1. Introduction

Effective lubrication and wear protection at high temperature and in cyclic environments are continuing challenges and have gained interest in different field of the industry. Oils and other liquid lubricants are now dominating the field of lubricated parts. However, concerns regarding pollution prevention and weight minimization have rushed incentives for the advancement of solid lubrication to replace, whenever possible, oils and their circulation systems. Solid lubricant coatings such as diamond like carbon (DLCs), transition metal dichalcogenides (TMD), and WC/C have been used to improve the performance and lifetime of different tribological components, such as cutting tools. However, their tribological properties degrade in humid atmospheres and/or at elevated temperatures due to their low oxidation resistance. To overcome this shortcoming, a new concept of lubrication has been proposed. Presently, self-lubricant coatings have been developed by combining the intrinsic properties of some binary and ternary coating systems, that are resistant to oxidation, with some elements that diffuse to the surface as a metal (e.g. Cu, Au, Pb, and Ag) and/or forming oxides (e.g. V_2O_5, $Ag_2Mo_2O_7$) and fluorides (e.g. CaF_2, BaF_2, and CeF_3) to get the lubricious properties. [1-2]. In all the cases, the main difficulty is the control of the lubricious metal diffusion to the surface, to achieve long term lubrication.

Researchers have been investigating various hard coating designs, which combine wear resistance and high temperature lubrication, to withstand harsh conditions. Self-adapting surfaces which provide lubricating effects at elevated temperatures can be used to reduce friction and improve wear resistance at such operating conditions. Using self-lubricious coatings that are based on formation of lubricious oxides, particularly Magnéli oxide phases has been proposed to achieve lubrication at elevated temperatures. Magneli phases are oxygen deficient homologous series, with general formula Me_nO_{2n-1}, Me_nO_{3n-1}, or Me_nO_{3n-2} which consists of a crystalline structure based on rutile structure. More recently, studies have focused on understanding the tribological properties of various homologous series of Magnéli phases (such as WOx, VOx, MoOx, and TiOx) which possess thermal stability in a wide temperature ranges and contain planar lattice faults that result in crystallographic shear planes with reduced binding strength [3].

Magneli phases of V containing (V_nO_{3n-1}) hard coatings are reported to show interesting tribological behaviours in the range 500 – 700 ^oC [2-5]. Since the original V containing hard coatings oxidise at high temperatures, the formation of lubricious V oxides on the coating surface at elevated temperatures enables them to reduce friction and control/avoid an increase in temperature caused by high friction. The layered structure of V_2O_5 and lower decohesion energy of these planes makes it mainly responsible for reduction of friction coefficient (COF) at elevated temperatures of V containing hard coatings. This easy crystallographic shearing of planes gives rise to the potential use of V_2O_5 as solid lubricant [6]. It can also act as a liquid lubricant at temperatures exceeding its melting point (670 - 685°C) [7-8].

The addition of vanadium on many binary and ternary coatings was reported to successfully reduce friction at elevated temperatures. However, such improvements were of short duration due to the rapid release of vanadium. This quick out diffusion of V from the bulk coating results

in the consequent loss of the low friction properties after few minutes [9]. The control of V out-diffusion is now one of the major challenges to achieve a suitable – long lasting wear and friction properties without compromising the original properties of the host binary and ternary films. Therefore, one possible proposal to solve this problem is to use coating systems with a dual phase structure, such as the case of TiSiN system, in which one of the phases (a-Si_3N_4) could act as a diffusion barrier to the lubricious phase metal (V) release [10].

1.1. Objectives

The main purpose of this thesis is to study the effect of V addition on the structure, mechanical properties, and tribological behaviour of Ti-Si-V-N films deposited by high power impulse magnetron sputtering (HiPIMS) in deep oscillation mode (DOMS). This coating (TiSiVN) has a potential to be used for high temperature lubrication applications where there are high demands, such as machining and aerospace industry. TiSiN system was selected because of its very high oxidation resistance similar to TiAlN, and TiCrN but with a much better mechanical properties [11]. Furthermore, if deposited in a nanocomposite structure (nano –size SiN grain embedded into a TiN matrix) or a multilayered structure (SiN layers alternated within TiN layers), the a-SiN phase can work as a diffusion barrier [10] (V diffusion is much slower in the amorphous Si_3N_4 than in TiN). In this work DOMS power supply was used to produce the TiSiVN films, as it has been reported to allow easier tailor the nanocomposite structure of the TiSiN films [12]; condition necessary to produce films with proper barrier to the lubricious species to achieve long term lubrication.

TiSiVN films were deposited using HiPIMS in DOMS mode with different vanadium content, silicon content, and peak power to study their effect on the structural, mechanical, and tribological behaviour of the coatings. TiSiN films were also deposited using the same conditions to be used as a reference. Chemical composition analysis was done using energy dispersive x-ray spectroscopy (EDS), surface morphology using scanning electron microscope (SEM), microstructure by x-ray diffraction (XRD), hardness and Young's modulus by nanoindentation. Scratch tests were performed to evaluate the adhesion of films to the substrate. Reciprocating sliding tests were carried out using alumina balls as a counterpart at room temperature to study the tribological behaviour.

1.2. Thesis structure

This thesis entitled "The effect of V content on the structure, mechanical properties, and tribological behaviour of Ti-Si-V-N films deposited by HiPIMS in deep oscillation magnetron sputtering (DOMS) mode " was done as a requirement to complete the joint master programme in tribology of surfaces and interfaces (TRIBOS).

The thesis is divided into five chapters. Chapter I is the introduction, describing the objectives and structure of the thesis. In Chapter II, the limitations of widely used liquid and solid lubricants at elevated temperatures, and the potential application areas of TiSiVN coating in the industry are assessed. The development of self-lubricious oxide coatings and the current knowledge and understanding of vanadium based coatings, particularly Ti-Si-V-N coatings are described in detail in state of the art (Chapter III). The materials and methods used for making the deposition as well as the techniques used for characterizing the coating are explained in

Chapter IV. Results and discussion are presented in Chapter V. Pin on disc tribological tests were also carried out on these coatings at room temperature and the results were published on VIII Iberian Conference on Tribology proceedings. This paper is attached as Annex A.

Chapter II

2. Industrial problem

Friction and wear reduction remain technological challenges from prehistoric times to modern days. Liquid lubricants and metal working (cutting) fluids are used in large quantities to provide lubrication and cooling effects during various metal cutting and forming processes. They improve energy transmission efficiencies by reducing friction and increase component life spans by reducing wear rates. These days, the use of these fluids is increasingly discouraged because of their harmful environmental effects.

ATC (Technical Committee of Petroleum Additive Manufacturers in Europe) has studied the environmental fate of engine lubricants and assessed product safety and health aspects in the 15 countries of the European Community (EU-15). Only in 2005 approximately 2,600 kilotonnes of crankcase lubricants were sold in EU-15 and it is estimated that 24% of lubricants leave the engine down the tailpipe as emissions of either combustion products or particulates. Nearly 75% of lubricants sold (2,000 kilotonnes) is drained as used oil and a very small amount (~ 0.5%) is lost as a result of leakage. Approximately 47% of drained oil is used as fuel oil or incinerated for energy value, while regeneration represents an estimated 24% of the total waste oil. The remaining 28% (730 Kilotonnes) of used oil is still unaccounted for and may be dumped into water and soil, or burnt entering the air compartment [13]. Figure 2.1 illustrates the proportion of lubricants pathways. Existing EU legislations concerning emissions to air, soil and water, and protection of workers tightly control the risk of exposure of lubricant (additives) to the environment and human being.

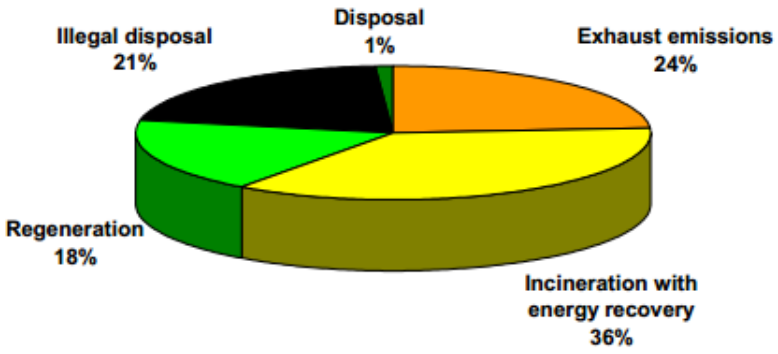

Figure 2.1. Fate of lubricants in Europe (adapted from [13])

Organisation for Economic Co-operation and Development (OECD) provides information on lubricants used in metal working (cutting) fluids, automotive lubricants, and hydraulic fluids. There are also significant releases from the sites where cutting fluids are used [14]. In addition to pollution, liquid lubrication also adds complexity to the system. Solid lubricants allow lighter and simpler equipment as they don't require lubrication distribution systems and seals.

Furthermore, when exposed to higher temperatures, most liquid lubricants will volatilize and fail to separate contacting solid bodies. This may lead to failure of the lubricated component and potentially other unrelated components when the vapour from the lubricant condenses or reacts on their surfaces. Lubricants also oxidize at high temperatures giving rise to the formation of lacquer, varnish, sludge, oil thickening, and most importantly corrosive wear. The oxidation products of oils at elevated temperatures can cause the formation and build-up of deposits at

interfaces that inhibit lubrication such as ring sticking. Moreover, in applications where the liquid can settle due to migration from aging leaving some parts unprotected liquid lubricants may not be appropriate. Solid lubricants are, therefore, utilized for high load and/or speed, extreme temperature, pressure, radiation, and reactive environment applications. To qualify as an effective solid lubricant, the friction coefficient (COF) has to be < 0.2 in most applications. For COF values bigger than 0.2, it is very likely for a plastic deformation of the contact surfaces to occur [15].

Wear should also be considered in addition to friction coefficient in the design of solid lubricants. Wear is the progressive loss of material at the surface of the body due to relative motion. Wear in sliding surfaces can be a result of one or more of the following main wear mechanisms; abrasive wear, sliding wear, chemical (corrosion) wear, adhesive wear, and fatigue wear [16]. Wear data are reported as 'wear rate' which is the total measured wear volume normalized by the load and the total distance travelled. For solid lubricants with moderate wear resistance, the typical wear rate values are between 10^{-6} and 10^{-5} $mm^3/N.m$ [15]. Since wear mechanisms and wear rate depend on the load and pass frequency (rate at which surface makes contact with counterpart), the application should be considered in materials selection. Solid lubricants are no different to this rule.

Aerospace industry (various satellite components, air foil bearings, and rolling element bearings), nuclear power industries (various furnace components, cylinder wall/piston ring lubrication for low-heat rejection diesel engines, as well as small arms action components), and other industries, such as material forming, tooling, military, and automotive, are some of the industrial applications with variable working conditions. For instance, the main challenge in high mach engine bearing (used in high performance aircraft) or high speed machine tool is to maintain the thickness of the lubricious layer. High-speed machine tools and air foil bearings for high mach aerospace engines are two examples of a particular interest to high temperature friction reduction with both involving different loading profiles. Air foil bearings are subjected to intermittent high loading and high pass frequency with times up to minutes prior to contacts for the bearings, while machine tools operate at relatively low loads with constant high speeds. These two applications are discussed in brief to illustrate what important principles have to be considered for high temperature solid-state lubrication.

2.1. High-speed and dry machining tools

Recently milling and cutting operations are making a transition to dry machining dictated by elimination of coolant media utilisation and circulation costs and environmental protection requirements. This shift in machining technology is supported by developments of thermally stable high temperature tool materials with hard and wear resistant surfaces. Rate of production in high speed machining is determined by tool speeds, feed rates and ultimately, interfacial temperatures between workpiece and tool. Even though oil-based coolants are used so often, coolant disposal can be a challenge to the environment. Incorporating sacrificial oxide formers (e.g. addition of Al to TiN) in hard coating materials to inhibit oxidation has been one method used to increase production rates [11]. This allows coating materials to possess stable mechanical properties at elevated temperatures. The properties of these coatings can also sometimes be modified further by adding one or more elements (e.g. V), which form Magnéli phases in dry machining operations where very high contact temperatures are common, to get additional properties of easy shear, thermal stability, and low adhesion.

For high-speed and dry cutting applications, high hardness and wear resistance in combination with low coefficients of friction or self-lubrication properties are required. Some of the factors that should be considered in developing high temperature solid lubricants for tool coatings and machines are hardness requirements, environmental robustness, and thermal stability. For cutting tools, hardness is the prime metric to ensure machining quality, tool life time, and reliable cutting. In machine contacts the contact load is usually distributed and contact fatigue is better avoided by using contact surface compliance; hence, does not normally require very hard mating contacts. Environmental robustness is very important as most machines have interrupted operations giving rise to regular and/or irregular temperature oscillations, exposures of various length and intensity to corrosion and oxidation. Stable operation is required for predicted and reliable operation of machine drive trains over the broad range of speeds, loads, environments, and temperatures. In addition to a stable operation at elevated temperatures, most of the mechanical contacts can experience a cold start followed by rapid heating or low/high temperature cycling during the operation. This requires the hard solid lubricated surfaces to have a stable friction coefficient over the broad temperature range and during temperature cycling. In dry cutting and high speed machining applications, lubricating mechanisms of the coating itself and low-friction are required in addition to excellent mechanical properties and structural integrity.

Minimising energy consumption during machining process by reducing friction is the main focus in most recent advancements in tool coating. The tribological effectiveness of intrinsic solid lubricants often starts to fail in humid environments, with increasing temperature, or due to oxidation [1]. Ongoing research efforts are trying to develop films that have an adaptive capability to form high temperature lubricious molybdenum, vanadium, and other Magnéli phase oxides. Currently, the use of solid lubricants for machine components is mostly limited to temperatures where structure evolution and contact oxidation are minimum (< 350 ^{o}C). Therefore, more work has to be done to expand the application of high temperature solid lubrication to general mechanical contacts such as gears, rails, and bearings.

2.2. The aerospace industry: air foil bearings

The aerospace industry presents particularly challenging lubrication problems since aerospace components operate under moist air, vacuum, low and high temperatures, a wide variety of environmental conditions. Driven by strict system weight reduction requirements, aerospace research and development centres were consistently investing in the development and exploration of high temperature solid lubrication. Application examples for high temperature solid lubrication in aerospace industry include lubrication of airfoil and hybrid bearings of jet engines, mechanisms for flight control surfaces of space-to-air re-entry vehicles and high mach planes, splines and bushings of jet, and rocket thrust vector controls [17]. High performance engines with improved efficiency could be developed if there were suitable lubricant materials that are effective over an extreme temperature ranges. Lubricants for satellites and space vehicles should be able to function in humid air as well as in vacuum. There is no single lubricant that is effective over such wide range of operating temperatures and environments. Therefore, a lubricant that can provide low friction and wear resistance from room temperature to high temperatures (~800^{o}C) or that operates on earth and in space would be a breakthrough and it would increase the performance and lifetime of the space vehicle. Oxides are promised to have the potential to lubricate in a wide range of environments, especially at elevated temperatures, and are being the focus of many researches [18].

Air foil bearings, which use air rather than oil, are self-starting bearings which rely on hydrodynamic air layer formed when the shaft is spinning above a critical rotational speed. Once the shaft, which is supported by a spring loaded foil journal lining, is rotating fast enough, the high pressure generated due to rotation pushes the foil away from the shaft so that there is no contact (figure 2.2). They have been used in the field of aeronautical engineering for air cooling machine (ACM), which is the main component to control temperature and pressure inside of aircraft cabins since 1970's. The air foil bearing has to be functional for a long term stable operation without maintenance and it is required to endure harsh environment, shock, and high speed. For example, foil bearings used for Boeing 747 operate for more than 100,000 hours without maintenance [19].

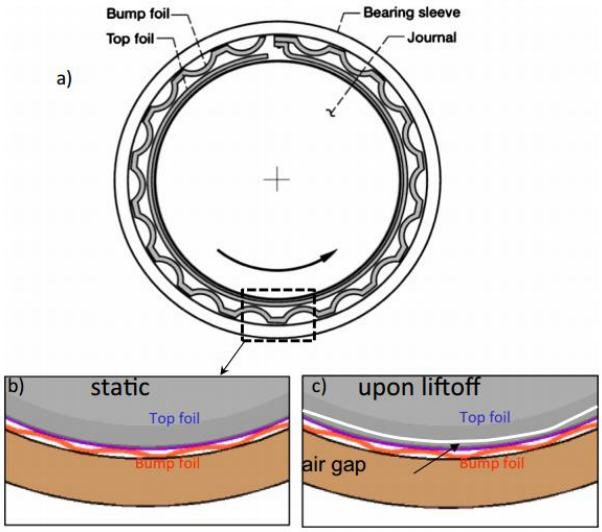

Figure 2.2. Schematic of air foil bearing [20]

Air foil bearings in high mach engines operate at 900ºC under high loads. The material should be lubricious over the entire temperature ranges experienced by the engine: from room temperature (at start up) to high temperature (during operation and shut down). All these demanding working conditions require the bearing to have thermal stability, as it will operate at high temperatures for long periods of time. Other applications for air foil bearings include high speed air cycle machines, turbo expanders, and bleed air turbo compressors [21].

In general, the growing attention of pollution prevention, the need for reducing the complexity of lubricating mechanisms, and demanding machining processes and aerospace industries requiring operations at extreme temperatures has encouraged advancement of solid lubrication and the development of novel tribological coatings with self-lubricating capability to replace, where possible, oils and their circulation systems. In many harsh working conditions especially with temperatures above 350°C, where liquid lubricants degrade rapidly, solid lubricants are the only viable alternatives to reduce friction.

Chapter III

3. State of the art

Solid lubricants can be grouped into carbon-based materials like diamond like carbons (DLCs), nanocrystalline diamond and graphite, soft metals (such as Ag, In, Sn, and Au), transition metal dichalcogenide compounds (WS_2 and MoS_2), inorganic fluorides (CaF_2, LiF, and BaF_2), metal oxides (PbO, B_2O_3, MoO_3, and NiO), and polymers (PTFE) [22-23]. They are applied either as fillers in self-lubricating composites or as surface coatings. Solid lubricants fall into either extrinsic lubricants that need the influence of an additive from the surrounding to activate the low shear mechanism (e.g. grahite), or intrinsic lubricants which have easily shearable atomic structure such as soft metals and MoS_2. The most widely used solid lubricants in industry such as MoS_2, graphite, and boron nitride have easy-shearing lamellar structure that results in low friction coefficient.

Most solid lubricants perform best in a narrow range of operating conditions. For instance, graphite, transition metal dichalcogenides, DLCs, and polymers lose their lubricating properties at temperatures exceeding 350ºC [17]. MoS_2 is an excellent lubricant in dry air environments or in vacuum but it degrades quickly in moist air. Graphite is the lubricant of choice for applications in dry or humid air but can't provide satisfactory results in vacuum. Polymers can only function in moderate temperature regimes. Fluorides (e.g. BaF_2, CaF_2, and CeF_3), soft metals (such as Cu, Ag, Pb, In, and Au), and some metal oxides (e.g. WO_3, V_2O_5) provide lubrication by forming easily shearing tribolayers at high temperatures. However, oxides are not lubricious at relatively low temperatures because they are typically brittle, form abrasive wear debris, and have high friction [18]. Fluorides become highly prone to cracking when used again at low temperature and can become glass-like after melting at high temperature. Table 3.1 summarises the temperature ranges achieved, and the benefits and challenges of typically used high temperature solid lubrication mechanisms.

Table 3.1. Comparison of currently used solid lubrication adaptive mechanisms [17].

Adaptive mechanism	Typical temperature range (in air)	Material examples	Benefits	Challenges
Structural transitions with hexagonal solid basal plane formation	< 300 ºC	MoS_2, WS_2, Graphite DLC ($sp^3 \rightarrow sp^2$) a-C, a-CH with metal carbides and nitrides MoS_2-$Sb2O_3$-graphite MoS_2-Sb_2O_3 MoS_2 encapsulated in oxides and nitrides	• Lowest friction and wear rates • Lowest cost options (burnishing)	Oxidation at higher temperatures
Diffusion of soft metals to contact surface	300 – 500 ºC	Ag and Au encapsulated in ZrO_2, Al_2O_3, TiN CrN, VN, TaN, Mo_2N, NbN	• Oxidation stable • Temperature self-regulated	Fast diffusion to surface depletes metal lubricant reservoirs
Lubricious oxide formation at contact surface	500 – 1000 ºC	Magneli phases: -V_2O_5, MoO_3, TiO_2 -WO_3, PbO, ZnO Double oxides: - silver molybdates - silver vanadates - silver niobates - silver tantalates Silicate glass forming: - Sc_2MoOS_3 - Cs_2WOS_3	• Provides liquid lubrication • very low friction • Environment supplies oxygen • Wear track self-healing • Some (glasses) use counter-part to form lubricant	Abrasion at low temperatures Lubricant extrusion from contact by the load

Various research groups are doing experimental studies on the formation of self-lubricating hard tribological coatings. Coatings with self-lubricating capability are appealing not only for demanding manufacturing operations and aerospace applications but also for rolling and sliding bearings in a wide range of tribological applications. Therefore, there is a significant pressing for the development of self-lubricating coatings. The challenge is to develop a hard self-lubricated coating that combines low contact friction, low wear rate, and addresses thermal management issues. Since Magneli oxides (with some exceptions) are often thermodynamically/chemically and structurally stable, they are believed to be potentially the best choice for solid lubrication in harsh conditions including extreme temperatures.

3.1. Lubricious oxide coatings

Coupled with other recent surface engineering strategies for high temperature contact, the progress in the design and exploration of hard coatings with high temperature adaptive behaviour opens a huge opportunity for adaptive coating applications on machine parts where oils and coolants are commonly used. Adaptive tribological coatings are materials that adjust their surface structure and chemical composition as a function of changes in the working environment to minimize friction and/or wear between contact surfaces. The adaptive mechanisms include thermally and mechanically induced phase transitions in hexagonal solids, metal diffusion and formation of lubricant phases at worn surfaces, formation of easy to shear solid oxides, contact surface tribo-chemical evolutions to form phases with low melting point, and others. To determine which coatings have a potential to be used as solid lubricant at elevated temperatures, it is necessary to understand the main mechanisms that lead to the reduction of friction and/or wear in high temperature.

Some of the mechanisms that result in lubricity, enhanced mechanical and tribological response observed for binary and ternary oxides at elevated temperatures include: easy shearing due to screening of cations by surrounding anions (crystal chemical model) [24]; creation of lamellar crystal structure materials with weak inter-planar bonds (similar to the shearing mechanism that occurs in graphite and MoS_2); melting of the oxide (similar to the mechanism that reduces friction in liquids) when working temperature is above melting point (Tm); shearing in textured nanocrystalline grains due to dislocation glide; and material softening (similar to the lubricious behaviour observed for soft metals) which occurs when the working temperature is between 0.4Tm – 0.7Tm that corresponds to the brittle-to-ductile transition of most oxides [20].

At moderate temperatures (300 – 500 ^{o}C), noble metals in the hard nanocomposite can be used to provide lubrication at contact areas by metal diffusion to the coating surface. However, reduction in mechanical stability of coating matrix, excessive contact deformation at elevated temperatures, and non-reversibility of the diffusion process important for temperature cycling are some of the shortcomings. Combining oxide chemistry adaptation and controlled metal/oxygen diffusion by insertion of diffusion control layers/phases is shown to be promising for lubrication at elevated temperatures. This makes the coating immediately below the diffusion barrier to be in as deposited condition and ready for adaptation upon exposure to the surface by the wear process [25].

High temperature lubricant coatings need to have structural and compositional stability. Many oxides exhibit thermodynamic stability up to 1000 ^{o}C and above but their strong ionic or covalent bonding makes their surfaces difficult to shear. This gives microcrystalline and single crystal oxides a characteristic abrasive and brittle nature at low temperature. However, the friction coefficient decreases with an increase in temperature and some oxides actually become

lubricants at high temperatures as a result of oxide softening or by control of defect structure and grain size [20]. To improve the tribological applicability of oxides, scientists have focused on developing nanocomposite and multilayer coatings with thin oxide layers formed on the coating surface (mainly by high temperature tribo-oxidation) for friction control while the bulk coating remains in non-oxidised state and provides load support and fracture toughness.

Incorporating metals that can form Magneli phases during operation to achieve lubricity in hard coatings has been the focus of several researchers. Magnéli phases are substoichiometric, homologous series compounds of certain transition metals with the formula Me_nO_{2n-1}, Me_nO_{3n-1}, or Me_nO_{3n-2} which were first discovered by Arne Magnéli in 1954. They contain planar lattice faults that result in easy shearing crystallographic planes which enhance the lubricity at elevated temperatures. More recently researchers are working to understand the tribological properties of various homologous series Magnéli phases like, TiOx, VOx, WOx, and MoOx [20].

Erdemir [24] developed a crystal chemical model that takes into account ionic potential to predict the low shear, and hence low friction behaviour of binary oxides. This model is based on the premise that the higher the ionic potential, the greater is the extent of screening of a cation of an oxide by surrounding anions. This gives rise to a soft and easy to shear (low friction coefficient) tribofilms. Figure 3.1 illustrates a close correlation between the ionic potential and friction performance of various oxides. Oxides with higher ionic potentials such as Re_2O_7, V_2O_5, and WO_3 provide low friction coefficients at elevated temperatures. On the other hand, oxides such as Fe_2O_3, MgO, and Al_2O_3 with lower ionic potentials, which has free cations that form strong ionic or covalent bonds are very strong and difficult to shear even at high temperatures.

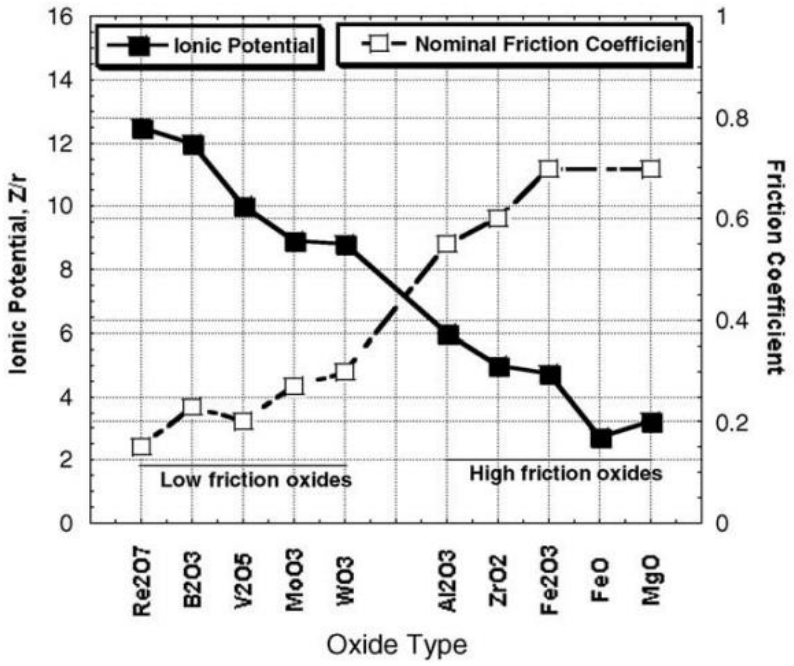

Figure 3.1. Relationship between ionic potentials and averaged friction coefficients of various oxides [24].

Incorporating sacrificial oxide formers (e.g. addition of Al to TiN) in hard coating materials to inhibit oxidation has been one method used to allow coating materials possess stable

mechanical properties at elevated temperatures. Addition of one or more element, such as vanadium that form Magnéli phases at high temperatures (> 600 °C), can sometimes provide easy shear and thermal stability by modifying the properties of these thin coatings. [26].

3.2. Vanadium based coatings

Several publications can be found in the literature on the formation of lubricious oxides that showed improvement in the friction and wear behaviour of coatings as a result of tribo-oxidation based on Ti, V, Mo, W, and Si. Lugscheider *et al.* [27] deposited a range of tungsten and vanadium-oxides by sputtering and ion plating processes onto dissimilar substrates (e.g. high speed steel, tungsten carbide, etc.). They reported that these coatings show good tribological properties and are promising to be used as solid lubricant films at elevated temperatures. In the last years vanadium rich films have been introduced as possible candidates for self-lubrication at high temperatures, mainly due to formation of easy shearing V_2O_5 oxide [28].

The principal oxides of vanadium occur in the form of VO, V_2O_3, VO_2, and V_2O_5 as single valence in oxidation states from V^{2+} to V^{5+}. The vanadium-oxygen phase diagram also includes mixed valence oxides containing two oxidation states with V^{4+} and V^{5+} such as V_6O_{13} and a series of triclinic Magneli phase oxides V_nO_{2n-1} (with n = 4 – 8, such as V_6O_{11}, V_7O_{13}, V_8O_{15}) which contain V^{4+} and V^{3+} species that are located between VO_2 and V_2O_3 (see figure 3.2)[29].

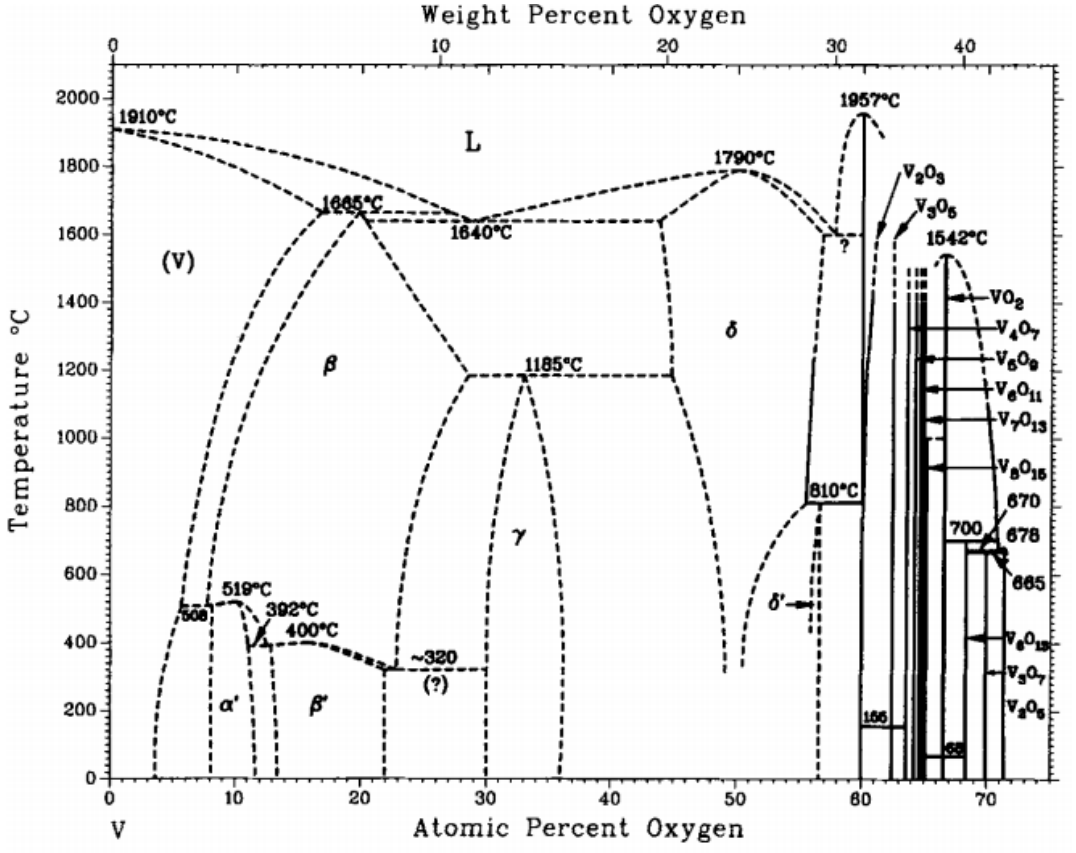

Figure 3.2. O-V phase diagram (condensed system, 0.1MPa) [29]

V_2O_5 has an orthorhombic crystal structure, which is its most stable configuration, with the lattice parameters a = 1.1510 nm, b = 0.4369 nm and c = 0.3563 nm and space group of Pmnm [30]. It is composed of distorted square pyramids which share corners and edges resulting the

formation of layer like structures parallel to the (001) plane as shown in figure 3.3. The bonds within the layers are strong while the interlayer binding is long-ranged and weaker and for this reason the material is easy to cleave in the plane perpendicular to c [31]. The layered structure of V_2O_5 and lower decohesion energy of these planes makes it responsible for reduction of friction coefficient (COF) at elevated temperatures of V containing hard coatings by acting as a solid lubricant. It can also act as a liquid lubricant at temperatures exceeding the melting point (670 - 685°C) [29].

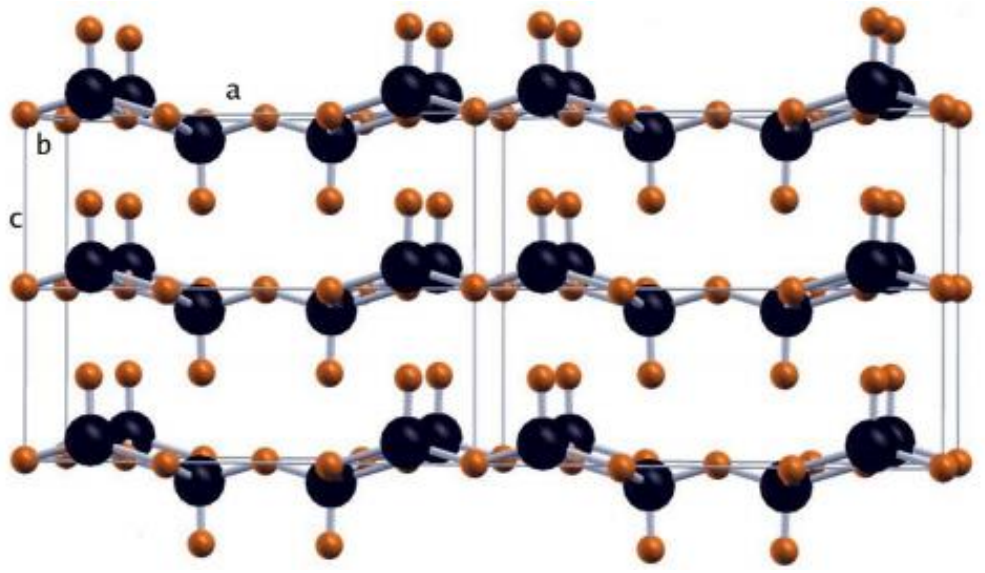

Figure 3.3. Illustration of V_2O_5 layered structure. The black spheres are V atoms and the small spheres are the O atoms [6].

Gassner *et al.* [7] observed a decrease in friction for binary VN hard coatings at elevated temperatures up to 700ºC due to the formation of V_2O_5 and other Magnéli phase vanadium oxides from V_nO_{2n-1} series. Even though the rapid oxidation of VN at higher temperatures provides lubricating effects, it is reported that it deteriorates the wear resistance and mechanical stability. Therefore, incorporating V to the state of the art hard coatings looks promising for low friction industrial applications. However, the developed coatings must provide a combination of controlled V out diffusion and mechanical integrity.

Various V based coatings have been developed such as multilayer TiAlN/VN [26], single layer TiAlVN [2,4,15], single and multilayer CrAlVN [32-33], and ternary (V,Ti)N [34], CrVN [35-36] and multi-layered AlN/VN [37], and TiSiVN [5]. TiAlVN coatings which combine the lubricating effects of vanadium oxides formed between 500 and 700ºC and superior mechanical properties of $Ti_{1-x}Al_xN$ phase are potential candidates for dry machining applications. The main disadvantage of this coating is the high friction coefficient (0.8 – 1.1) against steel. Kutschej *et al.* [4] evaluated the influence of the oxides formed on the friction behaviour of TiAlVN using high temperature ball-on-disc tests up to 700ºC. They reported a relatively low friction coefficient (0.27) between 500ºC and 700ºC. However, longer exposure time at elevated temperature resulted a slight increase in COF due to the reduction of V_2O_5 to other vanadium oxides with higher melting points. It has also been reported that VN in TiAlN/VN superlattices easily oxidizes at elevated temperatures and forms V_2O_5 having lubricious properties. Mayrhofer *et al.* [26] investigated the effects of vanadium oxides on tribological properties of

TiAlN/VN superlattices at high temperatures and reported friction coefficients as low as 0.18 at 700ºC (liquid V_2O_5 oxide) performed on dry sliding tests. Similar reduced friction and wear were obtained for AlCrVN [38]. All these results confirm the importance of vanadium addition and the presence of V_2O_5 to provide lubricious effects at elevated temperatures. However, this lubricious effect lasts only for a short duration due to a strong out diffusion of vanadium. Coatings deposited in nanocomposite or multilayer structure can be used to control the out diffusion of V with one of the phases acting as a diffusion barrier.

3.3. Ti-Si-V-N coatings

The addition of V on many binary and ternary coatings successfully reduced friction (with reported COF values of 0.2-0.3) at elevated temperatures (500 ºC – 700 ºC) [2,36]. The effect of vanadium doping on titanium based ternary coatings such as TiAlN, TiCrN, TiSiN, etc, have been attractive for advanced hard coating materials due to their suitable oxidation resistance and high hardness. TiSiN system has a very good oxidation resistance similar level to TiAlN and TiCrN but with much better mechanical properties. Moreover, if deposited as a nanocomposite structure, i.e. with TiN grains embedded in a Si_3N_4 matrix, the Si-N phase could work as an anti-diffusion barrier [10]. Therefore, the study of V addition on TiSiN system (TiSiVN), which combines the unique mechanical strength and the rapid oxidation with self-lubricating properties, makes it interesting for high temperature lubrication applications, as it could allow to develop a coating with controlled release of the lubricious species.

Fernandes *et al.* [5] first reported the effect of V content on mechanical properties, coating structure, and oxidation resistance of quaternary TiSiVN coatings deposited by DC reactive magnetron sputtering (DCMS). In that study TiSi(V)N coatings with different silicon and increasing vanadium contents were produced to study the effect of V additions on their properties. In addition, TiN and TiSiN coatings were deposited for reference. Si and V additions to TiN and TiSiN systems, respectively, did not change significantly either the global type of columnar morphology or the diffraction peaks indexed to a crystalline fcc TiN-type phase. A shift of the diffraction peaks to higher angles was always observed with either Si or V additions, suggesting the placement of those elements in substitutional solid solution in the TiN lattice. Therefore, the required nanocomposite structure needed for the control of vanadium diffusion was not deposited. This was explained by the low deposition temperature together with low substrate ion bombardment, which did not provide the necessary mobility of the species for the nanocomposite formation in DCMS. In conventional DCMS, the majority of deposited species are electrically neutral and the control of energy and direction of sputtered flux is limited. Si and V incorporation in solid solution in TiN gave rise to a slight increase in the hardness, although, for the high contents an inverse trend was observed. In that paper [5], Si and V showed to have opposite effects in oxidation resistance of TiN coating. Incorporation of Si improved the onset oxidation temperature of TiN coatings which can be attributed to the presence of protective Si-rich oxide films which act as an efficient diffusion barrier against oxygen and metal ions thus protecting the surface from further oxidation. Whereas, the addition of V on films significantly reduced the oxidation onset temperature to 500 ºC regardless of the amount of Si content indicating the rapid out-diffusion of V ions through the oxide scale inhibited formation of continuous protective silicon oxide layer. TiSiVN reveals a lower onset point of oxidation of approximately 100 ºC than TiAlVN and CrAlVN coatings which have on oxidation onset temperature close to ~600 ºC [2]. While the onset of oxidation displayed in TiAlVN and CrAlVN coatings was explained by the reactions between V and protective oxides, Fernandes *et al.* [5] didn't detect a combination of vanadium with silicon or titanium oxide. The rapid

oxidation of V and the outwards diffusion of its ions through the oxide scale was suggested to be the reason for loss of oxidation resistance of TiSiVN coatings, as they demonstrated in their last publication [39].

Fernandes *et.al* [40] also examined the tribological properties of these coating at room temperature on a pin-on-disc equipment using Al_2O_3 and HSS balls as counterparts. V addition to TiSiN system successfully reduced friction and wear rate of the coatings. They found that the improvement of the tribological behaviour was related to the V_2O_5 formation on the worn surface of the coatings. In the previous papers of Fernandes *et al.* [5] the nanocomposite structure required to control the release of the lubricious agent was not achieved due to the lack of substrate heating. In fact, to get such structure it is necessary to have sufficient mobility of the adatoms, which is normally achieved by the heating of the substrate**.** Other deposition technologies, such as chemical vapour deposition and cathodic arc deposition, have been used to produce such nanocomposite structure. Recently, Oliveira *et al.* [12] have shown that High-Power Pulsed Magnetron Sputtering (HiPIMS) allows to deposit and tailor the nanocomposite structure of TiSiN by changing the relevant deposition parameters, namely target peak power of the power supply.

3.4. HiPIMS (DOMS) process

High-power Impulse Magnetron Sputtering (HiPIMS) also knows as High-power Pulsed Magnetron Sputtering (HPPMS) and Modulated Pulsed Power Magnetron Sputtering (MPPMS) are the two recently developed sputtering techniques/power supplies that allow to deposit coatings with better adhesion to the substrate, enhanced hardness, wear and corrosion resistance, as well as specific electrical and optical behaviour [41]. Both techniques are based on the use of pulsed, high peak target power for a short period of time to achieve high plasma density and get improved quality of sputtered films by generating a high degree of ionization of sputtered species. The application of higher target voltages and currents and lack of positive reversal voltage between the high power pulses in both HiPIMS and MPPMS facilitates arc generation, especially for highly insulating reactive film deposition. This requires more complicated electronics for arc handling. The use of voltage oscillation packages with short off-time periods instead of using short rectangular voltage pulses to modulate the peak power, named deep oscillation magnetron sputtering (DOMS), has been proposed and shown to allow virtually arc-free depositions for reactive deposition of insulating film [42].

DOMS has an advantage of providing substantial ionization of the sputtered material resulting in denser films, increased adatoms/ions mobility, and allow better control of the deposition flux (for example, by varying the target peak power and substrate bias voltage) as compared to DCMS. Increased number of metal ions means greater control of deposition flux in terms of energy and direction. Even though DOMS allows deposition of dense films with higher hardness and better quality, for high peak powers the deposition rate is lower than DCMS [43]. Since the electrical discharge power is not high enough in conventional DCMS, only very little of the sputtered material is ionised. Increasing the power density would increase plasma density and hence more sputtered material is ionised; however, it will eventually melt the target and lead to arc generation. In HiPIMS the average power is kept low enough by applying very high power in repeated, short pulses to keep the target temperature below the melting point. Existing sputtering system can be changed into HiPIMS by essentially changing the power supply.

As referred before, Oliveira *et al.* [12] demonstrated that HiPIMS working in deep oscillation mode (DOMS) allows depositing the TiSiN system as a nanocomposite structure. They showed

that the nanocomposite structure can be easily tailored by changing the applied target peak power. Increase of the peak power led to a decrease in the TiN grains size while the amount of Si-N phase was kept constant. Thus, in this thesis work, it is intended to study the influence of V additions on the properties of TiSiVN films deposited by DOMS, with the main emphasis on production of a nanocomposite structure that could allow achieve proper controlled release of the lubricious agent, and hence, promote long term lubrication.

Chapter IV

4. Experimental procedure

4.1. Materials and methods

The films were deposited onto polished high-speed steel (AISI M2, Ø 20 × 3 mm) substrate for mechanical properties measurements, Si (111) for surface cross section and structural analysis, stainless steel discs (Ø 20 × 1 mm) for residual stress measurements, and FeCrAl alloy for chemical composition evaluation. AISI M2 substrate (Ø 24 × 7.9 mm) were used as base material for tribological tests.

All coatings were deposited by DOMS (HiPIMS Cyprium™III plasma generator, Zpulser Inc.). DOMS was chosen because according to Oliveira *et al.* [12] the nanocomposite structure of the TiSiN system can be easily obtained and tailored by this process. DOMS uses pulsed, high peak target power for a short period of time to generate high degree of ionization of the sputtered species, and hence to achieve high plasma density without melting the target. It allows direct control of the sputtered flux by achieving high degree of ionization of the sputtered material. High mobility, and hence surface and bulk diffusivity of ions/atoms, as a result of high ionisation efficiency of DOMS, influences nucleation and growth process positively to produce dense films, smooth surface finish, and strong film-to-substrate adhesion [25]. There are packets of oscillations in each DOMS pulse. In each oscillation the voltage and current gradually increase to maximum values and then decay to zero. Increase of the peak current (Ip) increases the ionized fraction of the sputtered material, whereas increasing the peak voltage (Vp) results in an increase in energy of the species bombarding the film during the growth [42]. A schematic of typical I–V waveforms of a DOMS pulse is depicted in figure 4.1. This form of high power pulse helps to reduce arc generation. The main advantage of DOMS over DCMS is the ionization of the sputtered flux i.e. higher ions to neutral ratio which improves the reactivity of the deposited species. Further, it allows better control of the deposition flux.

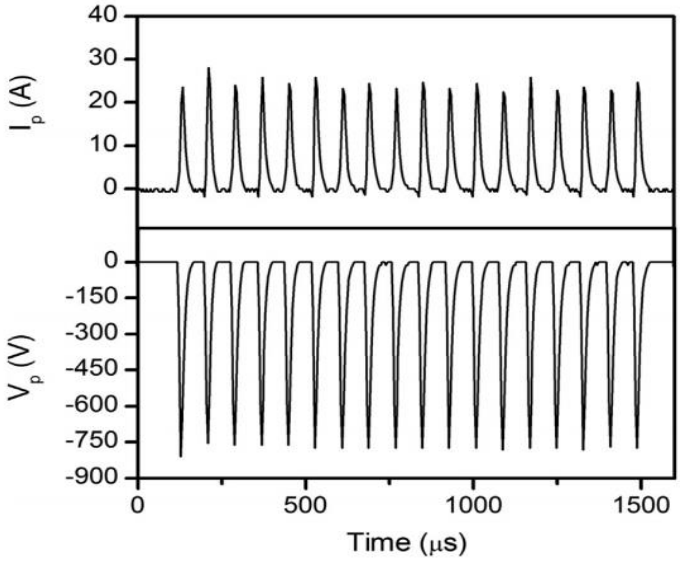

Figure 4.1. A typical I – V waveform spectrum in DOMS pulse [43].

4.2. Deposition procedure

All films were deposited in reactive mode by DOMS (HiPIMS Cyprium™III plasma generator, Zpulser Inc.). Prior to the depositions, all the substrates were ultrasonically cleaned in acetone and alcohol to reduce contaminations. The substrates were mounted in a rotating substrate holder (18 rev/min) with a target to substrate distance of 100 mm. A square (150 × 150 mm) high purity Ti (99.9%) target with 20 holes (10 mm in diameter) uniformly distributed throughout the preferential erosion zone was used (see figure 4.2). The holes were filled with different number of pellets of high purity Si (99.9%) and high purity V (99.9%) in order to achieve a desired Si and V content with the remaining holes filled with Ti pellets. A total of twelve depositions were made with two different silicon contents (7 and 11 pellets of Si). For each silicon content, three depositions with different vanadium content (0, 5, and 9 pellets of V) were made. All the above depositions were done twice with two different target peak powers (low and high peak power). The peak power (Pp), which is the average value of Vp*Ip calculated for each oscillation in a single pulse, was varied by changing the charging voltage (DC_{int}) of DOMS internal d.c. voltage source. DC_{int} of 240 V (Pp = 28 kW) was used for the low peak power. For high target peak power, DC_{int} of 300 V (68 kW) and DC_{int} of 350 V (109 kW) were used for coatings with 11 at.% Si and 7 at.% Si respectively. Pulse duration of 1500 µs, oscillation period of 80 µs and voltage on-time of 6 µs were used in this work.

Figure 4.2. Ti target with 20 holes uniformly distributed throughout the preferential erosion zone and filled with Ti, Si and V pellets in different configurations

Before making the deposition, the chamber was evacuated down to around 5×10^{-4} Pa. Ion gun composed of tantalum filament, a magnetic coil, and extraction electrode was used to clean the surface of the substrates. Using this equipment, the specimens were first heated by applying a positive voltage to the extraction electrode to drive the electrons to the main chamber and impinge on the surface. Substrate heating was performed in order to remove gases from the surface of the substrates, which can cause loss of adhesion. This step was followed by an "etching process" where Ar ions were extracted and impinge on the substrate. Much of the energy and momentum transferred from the bombarding ions becomes heat; however, some energy can be transferred to physically eject (sputter clean) surface atoms including contaminants. In both steps the energy was controlled by choosing a suitable bias (+80 V for substrate heating and -120 V for etching) to the substrate holder. Substrate heating and etching were done for 10 and 40 minutes, respectively before each deposition. All the films were deposited at a relatively high deposition pressure of 1.0 Pa using an Ar + N_2 discharge gas with

a P_{Ar}/P_{N2} ratio of 1/4. The peak power (Pp) applied to the target was varied in order to produce coatings with different microstructures. In order to keep the set average power (Pa) constant for each deposition, the pulse frequency (Fi) was automatically adjusted by the DOMS power supply software. The main deposition parameters used during deposition are compiled in table 4.1.

Table 4.1. Deposition parameters of the coatings

Coating	Number of Si pellets	Number of V pellets	DCint (V)	Pp (kW)	Pa (W)	Vp (V)	Ip (A)
TiSiN	7	0	240	28	600	844	33.6
TiSiVN		5					
		9					
TiSiN		0	350	110	1200	1110	98.0
TiSiVN		5					
		9					
TiSiN	11	0	240	28	600	844	33.6
TiSiVN		5					
		9					
TiSiN		0	300	68	800	1021	66.8
TiSiVN		5					
		9					

In order to improve the adhesion between the coating and the substrate, a TiSiV adhesion layer and TiSiVN gradient layer with increasing N content were deposited on the substrates before the final TiSiVN deposition. The deposition time was set in order to obtain a film thickness of approximately 1 μm excluding interlayer and gradient layers. The same was done for the reference TiSiN coating, with the only difference being V pellets replaced by Ti.

4.3. Characterisation techniques

Various test equipment were used for characterising the TiSiVN and reference TiSiN films. The chemical composition of the coatings were evaluated by energy dispersive spectroscopy (EDS). TiSiN films with different Si contents as measured by electron probe microanalysis (EPMA), from previous depositions, were used as reference for the EDS measurements. The thickness of the films were measured by profilometer supplemented with scanning electron microscopy (SEM) images. SEM was used to examine the fracture cross section and surface morphology of the coatings.

The crystallographic structure of coatings was investigated by X-ray diffraction (X' Pert Pro MPD diffractometer). Analysis in conventional ($\theta - 2\theta$) mode was performed in order to study the preferred orientation of the films. Further, grazing incidence x-ray diffraction (GIXRD) was carried out (using a grazing incidence angle of 3^o, scan range of $30^o < 2\theta < 80^o$, step size of 0.04^o, and Cu Kα1 radiation ($\lambda = 1.54060$ A)) to calculate the grain size and lattice parameters of crystallites. Pseudo – Voigt function was used to fit the XRD patterns for peak position (2θ) and full width at half maximum (FWHM) calculation. The lattice parameter was calculated by applying Bragg's law and geometrical relationship equation of lattice parameter with Miller indices and interplanar distance. Sherrer's equation was used for grain size calculation.

The deflection of the film-substrate body, measured both before and after deposition, with profilometer was used to calculate the level of residual stresses based on Stoney equation, which relates the curvature of the system and stress. Nano-indentation equipment (Micro Materials NanoTest), equipped with a Berkovich diamond pyramid indenter, was used for hardness and Young's modulus measurements, according to the method described by Antunes *et al.* [32]. A maximum applied load of 15 mN was selected to keep the indentation depth less than 10% of coating thickness in order to avoid the effect of the substrate. A total of 32 measurement, 16 indentations made at two different locations, were done for each coating.

The adhesion of the films was evaluated by scratch test apparatus using Rockwell C indenter with spherical tip radius of 0.2 mm by linearly increasing the normal load from 5 to 50 N (scratch speed of 10 mm/min) to generate a controlled scratch. A maximum load was limited to 50 N to prevent unnecessary wear of the stylus. Prior to testing, the samples and the indenter were cleaned with ethanol. Optical microscope analysis was used to determine the critical loads according to the standard for scratch test evaluation [44] . The critical load data was used to quantify the adhesive properties of the film.

The tribological behaviour of films were evaluated on a reciprocating sliding tribometer equipment in air, at room temperature, and relative humidity of 48 $\pm$5 %. The parameters used for the tribological test are 10N normal load, a frequency of 10Hz, 2 mm stroke, and 1200 cycles. Al_2O_3 balls of diameter 10 mm were used as counterparts. To ensure reproducibility of the results, three tests were done for each specimen under identical conditions. The specific wear rates were determined from the cross section area of the wear track using a Zygo – NewView 7200 3D optical profilometer. After tribological tests, the surface morphology and chemical composition of wear tracks and wear debris were characterised by scanning electron microscopy with energy dispersive X-ray spectroscopy (SEM – EDS). Raman spectroscopy was also used to analyse the oxides on the wear track.

Chapter V

5. Results and discussion

5.1. Chemical composition and deposition rate

The elemental chemical composition of the films obtained using EDS analysis is given in table 5.1. Regardless of the peak power, Si and V contents, the nitrogen content of the coatings was kept almost constant around 50%, showing that stoichiometric films were deposited. However, the Ti/Si ratio showed a significant variation when V was added. Depositions made using 7 and 11 pellets of Si gave an average 7 and 12 atomic percentage (at.%) Si. Depositions made with 5 and 9 V pellets had 6 and 11 at.% V content, respectively. No significant changes on Si and V contents were observed with increasing peak power in both series of Si rich coatings (7 and 12 at.% Si).

For easy coating identification, hereinafter the coatings will be designated as TiSixNz, or TiSixVyNz where x and y denote the Si and V contents in atomic percentage, respectively. Z denotes the target peak power used during deposition. Coatings designated with z = L represent depositions made at low peak power (28 kW) and z = H represent depositions made at high peak power (68 kW for coatings with 12 at.% Si and 109 kW for 7 at.% Si). The designation adopted for coatings identification is presented in table 5.1.

Table 5.1. Elemental chemical composition and designation of the coatings in at.%

Number of Si pellets	Number of V pellets	Coating designation	Chemical composition, at.%			
			N	Si	Ti	V
7	0	$TiSi_7N_L$	52.0 ± 0.5	7.1 ± 0.1	40.9 ± 0.5	
	5	$TiSi_7V_6N_L$	50.7 ± 0.5	7.1 ± 0.2	35.7 ± 0.5	6.4 ± 0.3
	9	$TiSi_7V_{11}N_L$	50.2 ± 0.5	6.8 ± 0.1	31.0 ± 0.4	12.0 ± 0.3
	0	$TiSi_7N_H$	52.0 ± 0.3	6.8 ± 0.1	41.2 ± 0.3	
	5	$TiSi_7V_6N_H$	51.2 ± 0.1	7.1 ± 0.1	36.0 ± 0.5	5.8 ± 0.3
	9	$TiSi_7V_{11}N_H$	50.6 ± 0.4	6.8 ± 0.1	30.5 ± 0.1	12.1 ± 0.5
11	0	$TiSi_{12}N_L$	52.4 ± 0.3	11.3 ± 0.2	32.3 ± 0.3	
	5	$TiSi_{12}V_6N_L$	52.0 ± 0.5	11.3 ± 0.1	30.5 ± 0.3	6.1 ± 0.3
	9	$TiSi_{12}V_{11}N_L$	52.0 ± 0.2	11.1 ± 0.2	26.8 ± 0.2	10.1 ± 0.7
	0	$TiSi_{12}N_H$	52.2 ± 0.3	12.2 ± 0.1	35.6 ± 0.3	
	5	$TiSi_{12}V_6N_H$	52.3 ± 0.6	13.0 ± 0.2	28.9 ± 0.1	5.8 ± 0.4
	9	$TiSi_{12}V_{11}N_H$	50.9 ± 0.3	14.3 ± 0.1	24.7 ± 0.6	10.1 ± 0.3

The target peak power was varied by changing the charging voltage (DC_{int}) of DOMS internal d.c. voltage source. As expected, an increase of the peak current (Ip) and peak voltage (Vp) was observed in both series of Si rich coatings (7 and 12 at.% Si) with increasing peak power (see table 4.1). According to Oliveira *et al.* [12] who studied the morphology and structure of TiSiN films deposited by DOMS, a linear evolution of the Vp and Ip in relation to the peak power was observed. When V pellets were added to the target, no changes on these parameters were noticed.

Table 5.2 displays the normalised deposition rate (i.e. deposition rate per kW of average power) for TiSi(V)N coatings with 7 at.% of Si deposited with the low and high peak power. Increase in the peak power in the DOMS discharge decreased the deposition rate of coatings (see $TiSi_7N_L$ and $TiSi_7N_H$ coatings). This behaviour is well documented in the literature and can be attributed to the combined effect of back attraction of metal ions to the target as a result of increased fraction of ionised sputtered flux (Ip) with increasing peak power, and due to sub-linear evolution of the sputtering yield with discharge voltage (Vp) [12,45]. Introduction of V pellets to the Ti target showed slight increase in the deposition rate of TiSi(V)N coatings. Although similar values of Vp and Ip were measured for the different series of Si rich coatings with V incorporation, according to the literature the sputtering yield of the VN is superior to that of the TiN, which justifies the increasing of deposition rate [46]. Similar evolution on the deposition rate was observed for coatings containing 12 at.% Si.

Table 5.2. Normalised deposition rate of TiSi(V)N films with 7 at.% Si

Coating	Deposition time (min)	Thickness (nm)	Normalised deposition rate ($nm.mm^{-1}.kW^{-1}$)
$TiSi_7N_L$	102	990	16.2
$TiSi_7V_6N_L$	102	965	15.8
$TiSi_7V_{11}N_L$	102	1010	16.5
$TiSi_7N_H$	100	997	8.3
$TiSi_7V_6N_H$	100	1020	8.5
$TiSi_7V_{11}N_H$	100	1063	8.9

5.2. Fracture cross section and surface morphology

The typical cross section morphology of the dissimilar films is shown in figure 5.1. Figures 5.1 a) to c) and d) to f) present SEM images of coatings containing 7 at.% Si deposited with low and high peak power, respectively. Whilst, figures 5.1 g) to i) and j) to l) are the cross section morphology of the coatings containing 12 at.% Si deposited with low and high peak power, respectively. All the films deposited using a peak power of 28 kW showed a fairly dense but columnar structure (figure 5.1 a – c, g – i) with columns extending from the substrate to the top of the film. However, films deposited with high peak power (109 kW (figure 5.1 d – f) and 68 kW (figure 5.1 j – l)) displayed a compact morphology, only with some very small remain columns observed. The columnar structure at low peak power can be attributed to the low energy of sputtered species and, hence low adatoms mobility of depositing species [5]. The film densification of coatings deposited at high peak powers is related to the increased ionised fraction of sputtered material (Ip) and increased energy of bombarding species (Vp), as both the peak voltage and peak current increased with increase in the peak power (see table 4.1) [42]. The energy provided at high Pp was enough to compensate the energy, which was lost due to high deposition pressure and lack of substrate bias.

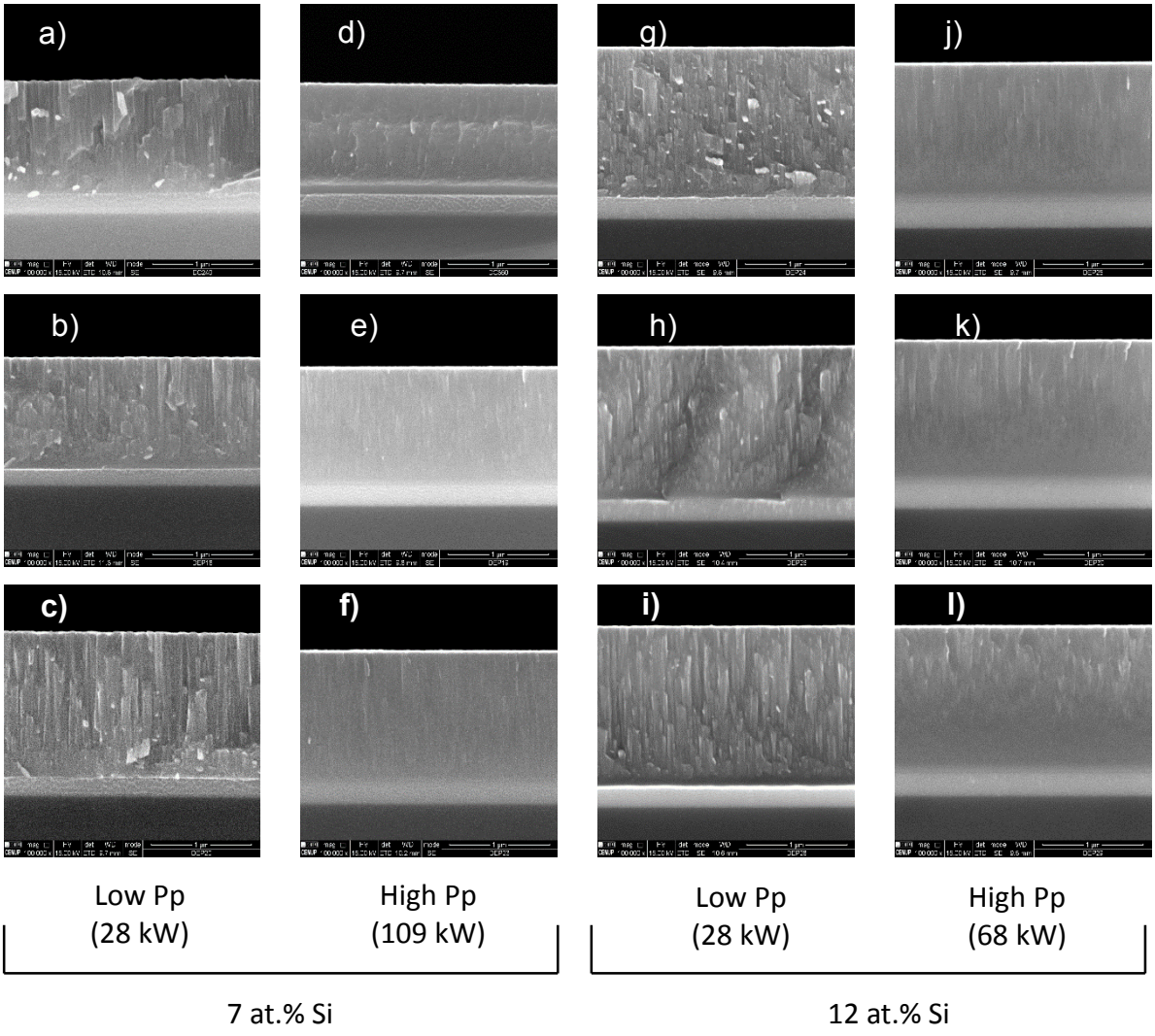

Figure 5.1. Fracture cross section of TiSi(V)N coatings: a) to c) and d) to f) coatings containing 7 at.% Si deposited with low and high peak power, respectively. g) to i) and j) to l) coatings containing 12 at.% Si deposited with low and high peak power, respectively. a) $TiSi_7N_L$, b) $TiSi_7V_6N_L$, c) $TiSi_7V_{11}N_L$, d) $TiSi_7N_H$, e) $TiSi_7V_6N_H$, f) $TiSi_7V_{11}N_H$, g) $TiSi_{12}N_L$, h) $TiSi_{12}V_6N_L$, i) $TiSi_{12}V_{11}N_L$, j) $TiSi_{12}N_H$, k) $TiSi_{12}V_6N_H$, and l) $TiSi_{12}V_{11}N_H$

The typical surface morphology of coatings is displayed on figure 5.2. Although the films were deposited using a rotating substrate which introduces anisotropy in the deposition system, top-view micrographs (figure 5.2) show that top of the columns have equiaxed geometry with no preferential elongation. The high fraction of ionised species supresses the deposition anisotropic geometry, as the substrate self-bias sensitive metal ions bombard the film at incident angles closer to the normal [12]. In fact, films deposited with low Pp have a cauliflower type surface morphology (figure 5.2 a – c, g – i), where grains aggregate to form larger structures. These types of structures are associated with unstable growth under surface diffusion limited conditions. On the other hand, coatings deposited with high Pp (increased surface mobility) exhibit granular morphology (figure 5.2 d – f, j – l) without any grain agglomeration. Such morphology is attributed to the increasing ions energy with Pp that bombards with more energy and efficiency the surface of the films. No significant differences were observed on the cross section and surface morphology of the coatings with V additions and silicon content.

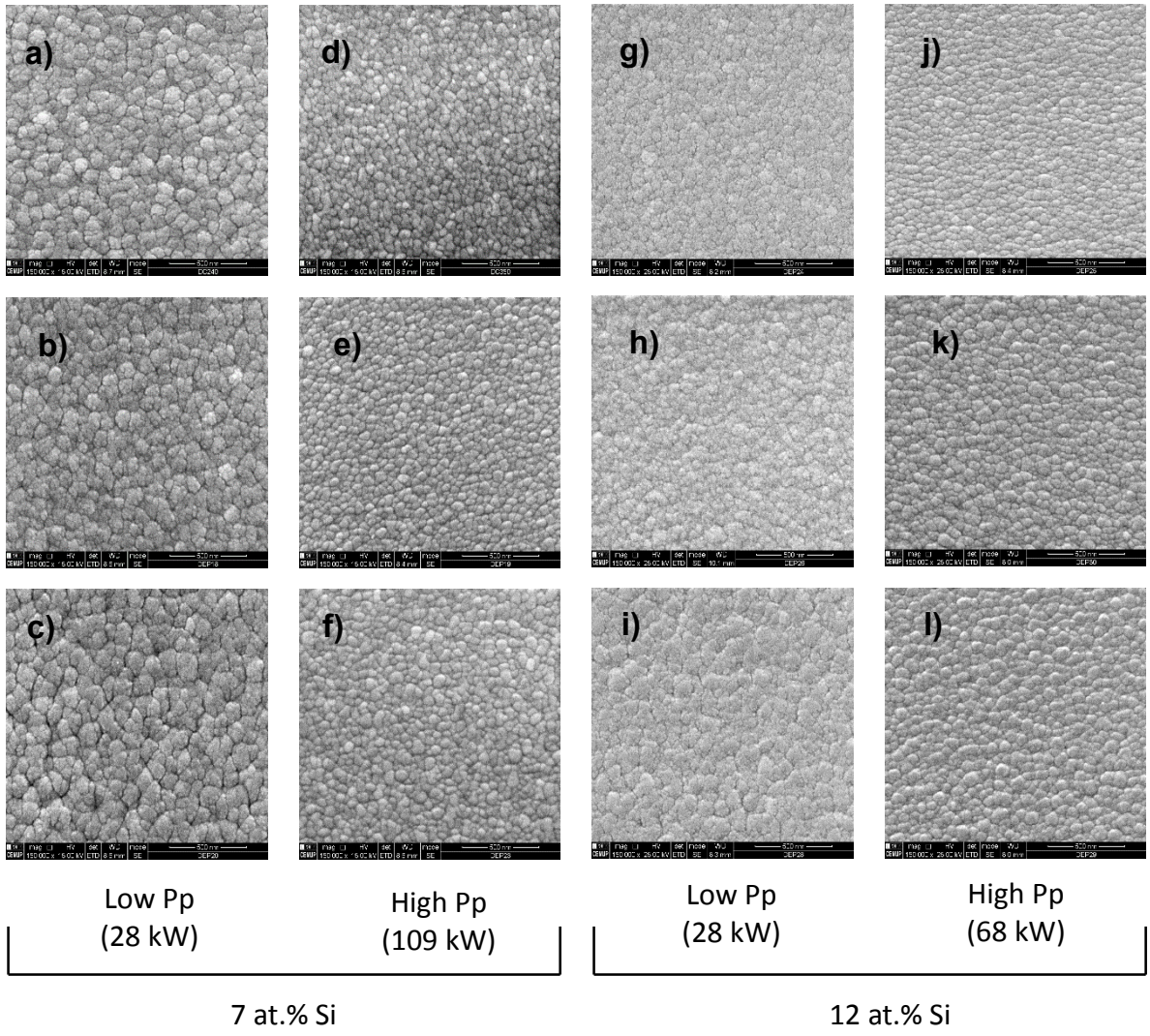

Figure 5.2. Top – view morphology of TiSi(V)N coatings: a) to c) and d) to f) coatings containing 7 at.% Si deposited with low and high peak power, respectively. g) to i) and j) to l) coatings containing 12 at.% Si deposited with low and high peak power, respectively. a) $TiSi_7N_L$, b) $TiSi_7V_6N_L$, c) $TiSi_7V_{11}N_L$, d) $TiSi_7N_H$, e) $TiSi_7V_6N_H$, f) $TiSi_7V_{11}N_H$, g) $TiSi_{12}N_L$, h) $TiSi_{12}V_6N_L$, i) $TiSi_{12}V_{11}N_L$, j) $TiSi_{12}N_H$, k) $TiSi_{12}V_6N_H$, and l) $TiSi_{12}V_{11}N_H$

5.3. Crystal structure (XRD)

The X-ray diffraction patterns of the TiSi(V)N coatings obtained in conventional mode are shown in figures 5.3 and 5.4 for coatings deposited with 7 and 12 at.% Si, respectively. All the coatings displayed diffraction peaks associated to the fcc NaCl type TiN phase (ICDD card no: 01 – 087 – 0633). No peaks associated with crystalline silicon nitride were observed. This is consistent with the reported formation of nc-TiN surrounded by amorphous SiN phase when TiSiN was deposited by HiPIMS as reported by Oliveira *et al.* [12]. Different peak positions, intensity, and broadening were observed depending on the vanadium content, silicon content, and peak power used. The effect of target peak power and V addition on the structure of the coatings with 7% at.% Si content is displayed in figure 5.3. Spectrums a – c) and d – f) display the effect of V additions on the structure of the coatings deposited with low and high peak powers, respectively. V additions shifted the diffraction peaks to higher angles, behaviour associated with smaller unit cell. Since similar levels of compressive residual stresses were measured for each series of the V rich coatings with respect to the references TiSiN films (see

table 5.3), this behaviour can only be explained by substitution of Ti by the smaller V atoms, which due to its smaller atomic radius promotes the contraction of the TiN lattice. This observation agrees well with the observations of Fernandes *et al.* [5] who studied the influence of V additions on the TiSiVN films deposited by DCMS [5] and Pfeiler *et al.* [15] who investigated the effect of V additions on the TiAlN system deposited by cathodic arc evaporation. Independently of the peak power used, the diffractions peaks become sharper and increased in intensity with increase in V content suggesting an increase in crystallinity.

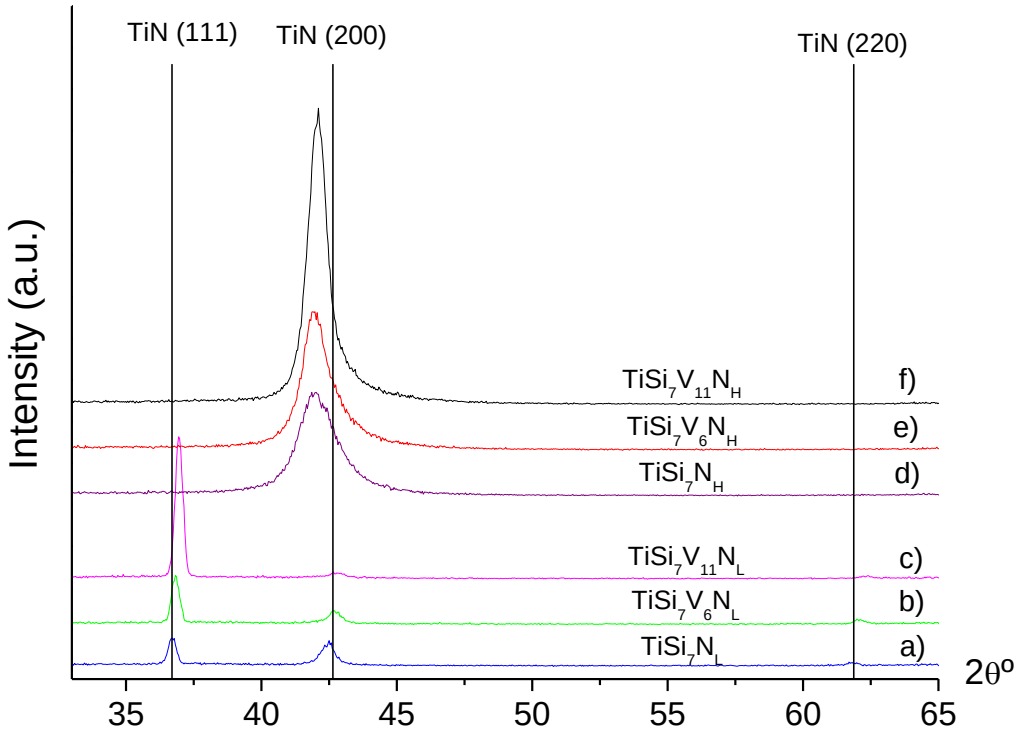

Figure 5.3. Effect of V content and target peak power on θ-2θ XRD patterns of TiSi(V)N coatings with 7at.% Si. a) to c) and d) to f) coatings deposited with low and high peak power, respectively. a) $TiSi_7N_L$, b) $TiSi_7V_6N_L$, c) $TiSi_7V_{11}N_L$, d) $TiSi_7N_H$, e) $TiSi_7V_6N_H$, f) $TiSi_7V_{11}N_H$

Films deposited with low Pp had (111) preferential orientation. This agrees with observations reported by Faz *et al.* [47, 48] and Chawla *et al.* [49] for TiN films deposited at low bombardment conditions with low ion-to-neutral ratio. For coatings deposited using high peak power, peaks (111) vanish indicating preferential growth in (200) orientation parallel to the substrate surface. The increased ion to neutral ratio (Ip) at high Pp in the bombarding flux increases adatoms mobility, favours (200) preferred orientation, and film densification. This change in preferential orientation is related to the surface energy [50]. If the energy of bombarding flux (Vp) is increased above critical threshold value, the incident particles will penetrate in the sub-surface of growing and will induce compressive stress and film defects as a result of atomic peening effect [51]. The TiN film grows in (200) orientation at high ion energies because it has more open ion channelling planes than the dense (111) planes which are destroyed during film growth [12]. Furthermore, (200) peaks exhibit peak broadening and lower intensity (particularly for TiSiN) with increase in peak power indicating smaller grain size (see figure 5.6) and reduced crystallinity. For instance, the grain size of $TiSi_7N$ (200) peak was reduced from 19 nm to 6 nm when the peak power was increased from 28 kW to 109 kW.

Moreover, in the films deposited using high peak power (figure 5.3, spectrums d-f), the diffraction peaks showed a shift to lower diffraction angles as compared to the position of the reference TiN and the coatings deposited with low peak power. This shift to lower angles can be associated with the increase of compressive residual stresses on the film with increasing peak power (see table 5.3). The level of compressive residual stress of coatings deposited at high peak powers is more than twice than those deposited at low peak power. This increase in residual compressive stresses can be explained by the increase of energy of bombarding ions when the peak power is increased, as reported elsewhere [51].

TiSiN films deposited with 12 at.% Si (figure 5.4) showed very low intensity and broad diffraction peaks with a (200) preferential orientation, even for coatings produced with low peak power. As stated before, at low peak powers the mobility of adatoms on the surface of the growing film is very low, and a (111) orientation would be expected. However, according to the literature for TiSiN films with Si content higher than 11 at.%, a (200) orientation have been always formed, even for situations of low adatoms mobility [49]. The low intensity of the diffraction peaks of these coatings could be associated with the lower degree of crystalline phase nitriding. As for coatings deposited with 7 at.% of Si, V additions shifted the diffraction peaks to higher angles. Since similar level of residual stresses were measured for these series of coatings, this behaviour is once again related to the substitution of Ti by V atoms on the TiN lattice. However, contrarily to the previous films, in the present case V additions showed to have an opposite behaviour on the peaks intensity i.e. decrease the [200] peaks intensity.

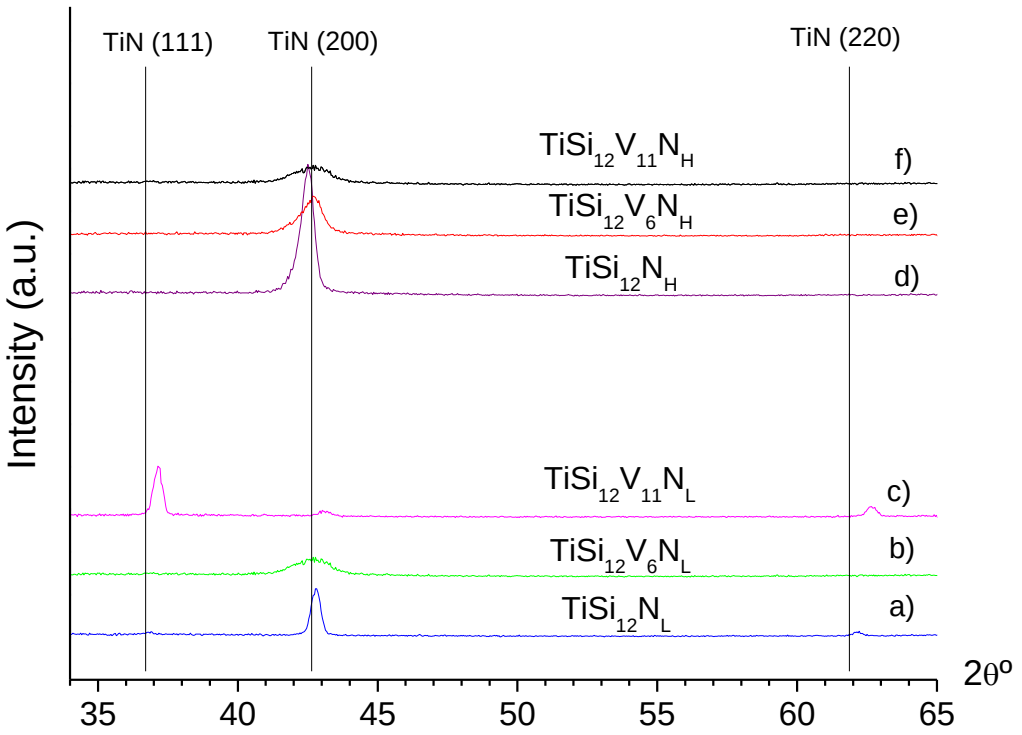

Figure 5.4. Effect of V content and target peak power on θ-2θ XRD patterns of TiSi(V)N coatings with 12 at.% Si. a) to c) and d) to f) coatings deposited with low and high peak power, respectively. a) $TiSi_{12}N_L$, b) $TiSi_{12}V_6N_L$, c) $TiSi_{12}V_{11}N_L$, d) $TiSi_{12}N_H$, e) $TiSi_{12}V_6N_H$, and f) $TiSi_{12}V_{11}N_H$

5.3.1. Lattice parameter

Figure 5.5 presents the lattice parameter of TiSi(V)N coatings calculated from the (200) difraction peak of the XRD patterns obtained in grazing incidence. Grazing incidence allows to detect grains in various orientations. XRD patterns of all coatings obtained in grazing mode can be found in Appendix B. From the figure, it can be easily seen that the coatings deposited at higher peak powers (both coatings with 7 and 12 at.% Si) have a slightly higher lattice parameter than the same series of coatings deposited with low peak power. This difference is much more notorious on the coatings deposited with low Si content, due to the higher peak power used. This result agrees well with the shift of the XRD diffraction peaks to lower angles, and can be attributed to the formation of high level compressive residual stresses with increasing the peak power. V additions to the reference TiSiN coatings decreased the lattice parameter of films almost linearly. Taking into account that the measured residual stress levels are similar for depositions made with the same Pp, the smaller lattice parameters are imputed to the formation of substitutional solid solution, i.e. replacement of Ti by V atoms in the TiN lattice.

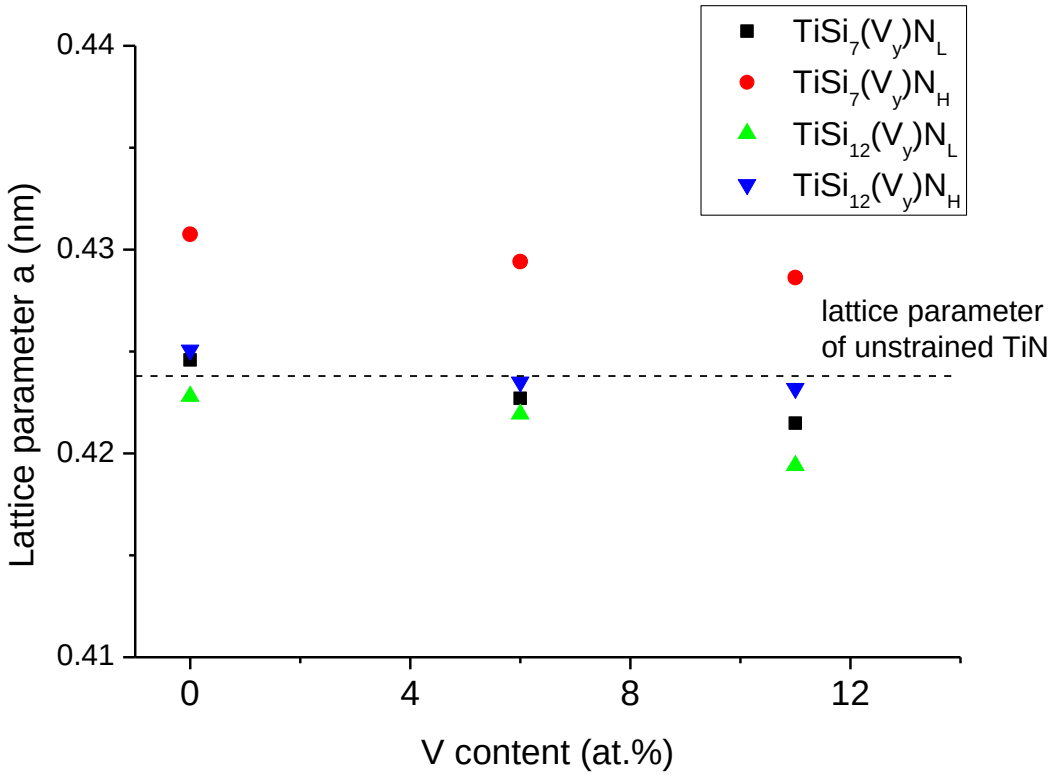

Figure 5.5. Lattice parameter of TiN (200) as a function of V content

5.3.2. Grain size

The effect of peak power on grain size is presented in figure 5.6 (a) for the coatings deposited with 7 at.% Si. Sherrer's equation, which relates the grain size to the broadening of the XRD diffraction peak, was used for grain size calculation. Films deposited at high peak powers exhibited smaller grain size than coatings deposited at low peak power, as shown in figure 5.6 (a). This behavior is attributted to the high ions energy achieved when high peak powers were

used, which bombardes the surface of the growing film more efficiently, creating a large number of nucleation points that limits the growth of the grain size. The average values of grain size decreased from 17 nm at low peak power to value of 8 nm at high Pp. Oliveira *et al.* [12] also reported a progressive decrease in the grain size of TiN (001) and (002) diffraction peaks from 25 nm to less than 5 nm with increase in peak power from 26 kW to 148 kW.

Figure 5.6 (b) illustrates the effect of silicon content on the grain size of (111) peaks for coatings deposited at low Pp. As can be seen in the figure, increasing the silicon content did not significantly influence the grain size of the coatings. Niederhofer *et al.* [52] also observed that grain size is almost independent on Si (Si_3N_4) content if the surface of the growing film is heavily bombarded by energetic ions during growth.

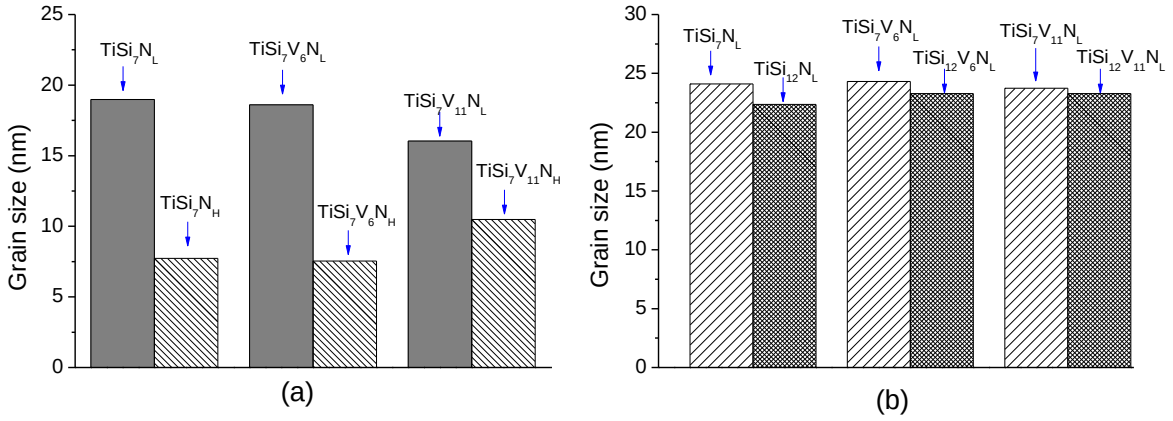

Figure 5.6. (a) effect of peak power (Pp) on grain size of (200) peak for TiSi(V)N coatings deposited with 7 at.% Si, (b) effect of Si content on the grain size of (111) peak the coatings deposited using low peak power (28 Kw) with increasing V content.

5.4. Mechanical properties

Table 5.3 presents the level of compressive residual stresses of the films deposited with different peak powers, containing 7 and 12 at.% Si, and with V additions. Stoney equation, which relates the curvature of the system and stress, was used to calculate the level of residual stress by measuring the deflection of the film-substrate body. All coatings are in compressive residual stress state regardless of peak power, Si and V content. The measured residual compressive stress is a combination of both intrinsic and thermal stress. Thermal stress is determined by substrate temperature and thermal expansion coefficient difference between the film and the substrate. The level of compressive residual stress for the coatings (both with 7 at.% Si and 12 at.% Si) deposited at high peak powers was more than twice than those deposited at low peak power. In fact, the compressive stress of samples deposited at high Pp increased by 1.03 to 2.36 GPa in comparison with respective stress values at low Pp. This could be mainly due to the intense ion bombardment (atomic peening) supporting the higher energy and ion generation in HIPIMS at high peak power [53]. Coatings with 12 at.% Si content showed a higher level of compressive residual stress (~ 11%) than those with 7 at.% Si. This could be a result of the presence of high amounts of Si_3N_4 which more efficiently enrobes the TiN grains and could create high levels of residual stresses. High level of residual stress may be beneficial to the hardness of the coating, but it is also detrimental to the fatigue and wear resistance of coatings, because it may cause adhesive as well as cohesive delamination in a coating. The addition of V seems to have almost no influence on the level of residual stress.

Table 5.3. Level of residual stress on the films

Deposition	Residual stress (GPa)	Deposition	Residual stress (GPa)
$TiSi_7N_L$	-1.96	$TiSi_{12}N_L$	-1.65
$TiSi_7V_6N_L$	-1.52	$TiSi_{12}V_6N_L$	-1.81
$TiSi_7V_{11}N_L$	-1.23	$TiSi_{12}V_{11}N_L$	-1.80
$TiSi_7N_H$	-2.99	$TiSi_{12}N_H$	-4.01
$TiSi_7V_6N_H$	-3.85	$TiSi_{12}V_6N_H$	-4.07
$TiSi_7V_{11}N_H$	-3.54	$TiSi_{12}V_{11}N_H$	-3.41

The hardness (*H*) and Young's modulus (*E*) of the different films are shown in figure 5.7. Coatings deposited at high peak powers showed higher hardness values than those deposited at low peak power. The higher hardness value of the coatings deposited with high peak power can be attributed to the combined effect of grain size refining of the nanocomposite structure (Hall - Petch effect), lower size of nano-columns in the film [54], and high level of induced biaxial compressive stress due to increased energetic ion bombardment during deposition [55] [56]. Hardness is directly correlated to nucleation and slipping of dislocations. The combined effect of typical lower dislocation density of small grains and increased grain boundary, which acts as an obstacle to dislocation flow across the grains, contributes to the increase of hardness during grain size refining. The maximum hardness achieved in this work was 31.6 GPa for $TiSi_7N_H$, which is a value much lower than those reported in the literature for similar Si content [52,57]. In fact, in such coating system, extremely high hardness values could be reached if a monolayer of a-SiN is involving the TiN grains. In the literature this is normally achieved for a Si concentration in the range of 5 – 10 at. % Si [57]. With further increase in Si content, amorphous phase is expected to reduce the hardness and toughness of the films by allowing mechanical deformation i.e. the hardness of the nanocomposite approaches the hardness of Si_3N_4 [58-59]. Films with 12 at.% Si content didn't exhibit a significant decline in both hardness and Young's modulus as opposed to the reported decrease in hardness when Si content exceeds percolation threshold (5 – 10 at.%) [56, 60-61]. V additions to the TiSiN coatings generally decreased their hardness. This behaviour revealed to be independent of the peak power and Si content on the coatings.

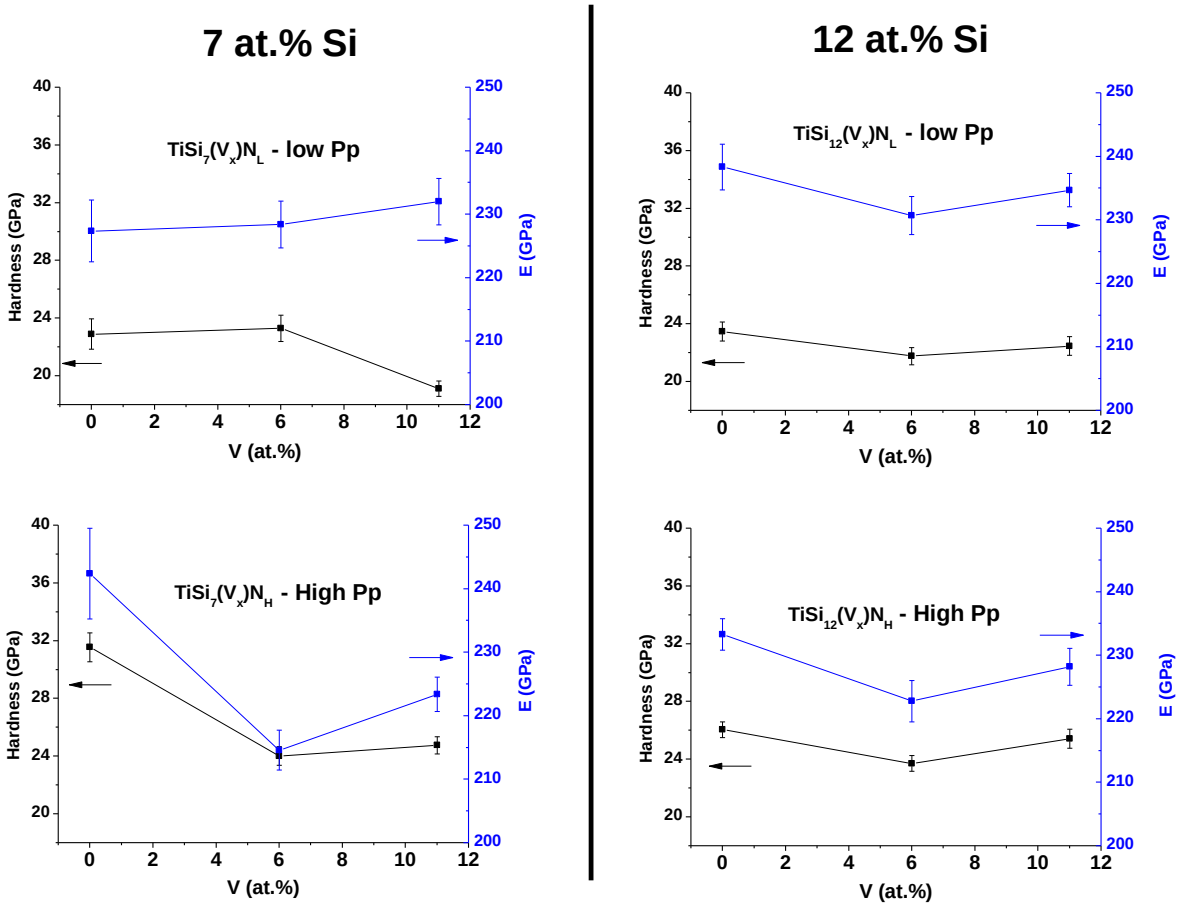

Figure 5.7. Hardness and Young's modulus values of the coatings vs V content

5.5. Scratch adhesion test

Strong adhesion of the film to the substrate material is crucial for long lasting mechanical and tribological applications because adhesion determines the film's endurance life and load bearing capacity. Low stress and stress gradients, high fracture toughness of materials, non-planar defects, low concentration of flaws, interfacial roughness that necessitates propagation direction change, and presence of fracture blunting features promote good adhesion. On the contrary, high residual film stresses, low degree of bonding (low nucleation density), low fracture toughness (brittle materials, flaws), and/or poor interfacial contact may cause poor adhesion.

The typical coating failures, observed in the scratch tracks of the different coatings, are presented in figure 5.8. After post-observation by optical microscopy, the information for the critical load was collected with respect to the first chipping (Lc2), coating delamination within the track or large area coating chipping (Lc3) [62]. The summary of the critical loads Lc2 and Lc3 is given in table 5.4.

Figure 5.8. Scratch track morphologies of coatings in as deposited condition: a - c) and d to f) coatings containing 7 at.% Si deposited with low and high peak power, respectively. g to i) and j to l) coatings containing 12 at.% Si deposited with low and high peak power, respectively. (a) $TiSi_7N_L$, (b) $TiSi_7V_6N_L$, (c) $TiSi_7V_{11}N_L$, (d) $TiSi_7N_H$, (e) $TiSi_7V_6N_H$, (f) $TiSi_7V_{11}N_H$, (g) $TiSi_{12}N_L$, (h) $TiSi_{12}V_6N_L$, (i) $TiSi_{12}V_{11}N_L$, (j) $TiSi_{12}N_H$, (k) $TiSi_{12}V_6N_H$, and (l) $TiSi_{12}V_{11}N_H$

According to figure 5.8, the failure mechanisms observed for most of the coatings can be characterised by an initial part of plastic deformation followed by appearance of small

conformal type cracks or edge chipping, and eventually substrate exposure with either discontinuous or continuous ductile perforation of the film.

$TiSi_7N_L$ (figure 5.8, a) started with conformal type buckling cracks at low loads followed by discontinuous ductile perforation and then continuous perforation of the coating with Lc2 value of 33 N and Lc3 at 40 N. On the other hand, $TiSi_7V_6N_L$ films exhibited edge chipping (cohesive spallation along the scratch borders) at a relatively low load of 10 N and substrate exposure at 36 N (figure 5.8, b). Neither edge chipping nor substrate exposure was observed for $TiSi_7V_9N_L$ (figure 5.8, c). $TiSi_7N_H$ (figure 5.8, d), $TiSi_7V_6N_H$ (figure 5.8, e), and $TiSi_7V_{11}N_H$ (figure 5.8, f) showed similar scratch behaviour with conformal type buckling cracks at low loads followed by discontinuous ductile perforation, and finally substrate exposure by continuous perforation of the coating with critical Lc3 loads of 45 N, 20 N, and 42 N, respectively. $TiSi_{12}V_6N_L$ (figure 5.8, h) exhibited gross interfacial shell-shaped spallation from the starting test load of 5N, suggesting poor adhesion between the film and the substrate. Cohesive spallation along the scratch borders without continuous substrate exposure was observed for $TiSi_{11}N_L$ (figure 5.8, g) and $TiSi_{12}V_{11}N_L$ (figure 5.8, i) with critical Lc2 load of 21 N and 16 N, respectively. All $TiSi_{12}N_H$ (figure 5.8, j), $TiSi_{12}V_6N_H$ (figure 5.8, k) and $TiSi_{12}V_{11}N_H$ (figure 5.8, l) coatings showed cohesive spallation along the scratch track borders and discontinuous ductile perforation. The corresponding Lc2 and Lc3 values of these coatings are presented in table 5.4. In general, most of the coatings are well adherent to the substrate exhibiting high Lc values. Comparatively, TiSiVN coatings with 6 at.% V showed poor adhesion properties. This behaviour can be connected with the observed low hardness of the films. Higher compressive stresses may have contributed for the relatively poor scratch behaviour of films deposited at high peak powers.

Table 5.4. Critical loads of scratch test

Coating	Lc2 (N)	Lc3 (N)
$TiSi_7N_L$	33	40
$TiSi_7V_6N_L$	10	36
$TiSi_7V_9N_L$	N/A	N/A
$TiSi_7N_H$	41	45
$TiSi_7V_6N_H$	15	20
$TiSi_7V_{11}N_H$	36	42
$TiSi_{12}N_L$	21	N/A
$TiSi_{12}V_6N_L$	N/A	N/A
$TiSi_{12}V_{11}N_L$	16	N/A
$TiSi_{12}N_H$	12	43
$TiSi_{12}V_6N_H$	11	29
$TiSi_{12}V_{11}N_H$	14	32

5.6. Tribological properties

5.6.1. Wear rate

The calculated specific wear rates of the coatings (deposited with 7 at.% and 12 at.% Si and with V additions produced with low and high peak powers) are shown in figures 5.9 a) and b). Different evolutions were observed depending on the Si and V contents present on the coatings and also on the peak powers used. Hereinafter, the wear rate on the coatings produced with 7 and 12 at.% Si will be discussed separately in order to better understand the effect of V additions and the effect of the peak power on their tribological behaviour. Increasing the peak power in the TiSiN coatings deposited with 7 at.% Si (figure 5.9, a) decreased the wear rate. Such behaviour is in good agreement with the increase of hardness (see figure 5.7) and improvement of compactness (figure 5.1, d) of the coating. TiSi(V)N coatings with 7 at.% Si (figure 5.9 a) deposited at low peak power showed a progressive decrease in wear rate with V addition. As it will be shown later, this can be ascribed to the presence of V-O lubricious phases on the wear track of the coatings which increased with increasing V content on the films. At high peak power, the wear rate of coatings first increased and then decreased with V additions. The first increase of wear rate with V addition ($TiSi_7V_6N_H$ coating) matches well with the low critical load values (table 5.4) and the high level of residual stresses (table 5.3) displayed by the coating. $TiSi_7V_{11}N_H$ deposited with high peak power showed the highest wear resistance among all the coatings.

Reference TiSiN coatings with 12 at.% Si showed lower wear resistance (figure 5.9, b) as compared to TiSiN coatings deposited with 7 at.% Si (figure 5.9, a). Increasing the peak power on TiSiN coating deposited with 12 at.% Si degraded the wear resistance of the coating. As it will be discussed later, this can be attributed to the high levels of compressive residual stresses on the coating which promotes a brittle behaviour. Coatings of this series deposited with 6 at.% V showed delamination. This behaviour was independent of the peak power used and can be attributed to the low critical adhesion load values displayed by these coatings (see figure 5.8 and table 5.4). Further increase of V additions decreased the wear rate of films. However, when compared with the coatings deposited with low silicon (7 at.%) content deposited with the same V amount, they displayed a slightly higher wear rate.

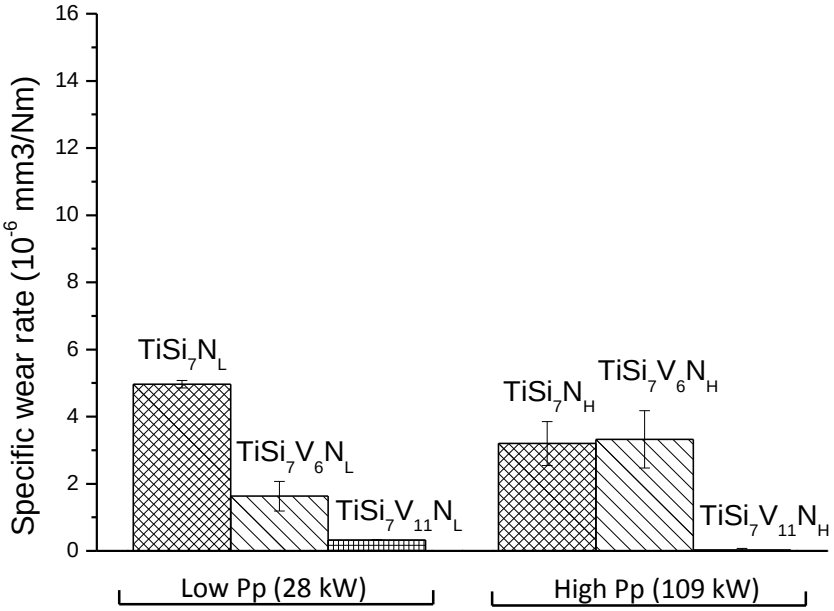

(a) 7 at.% Si

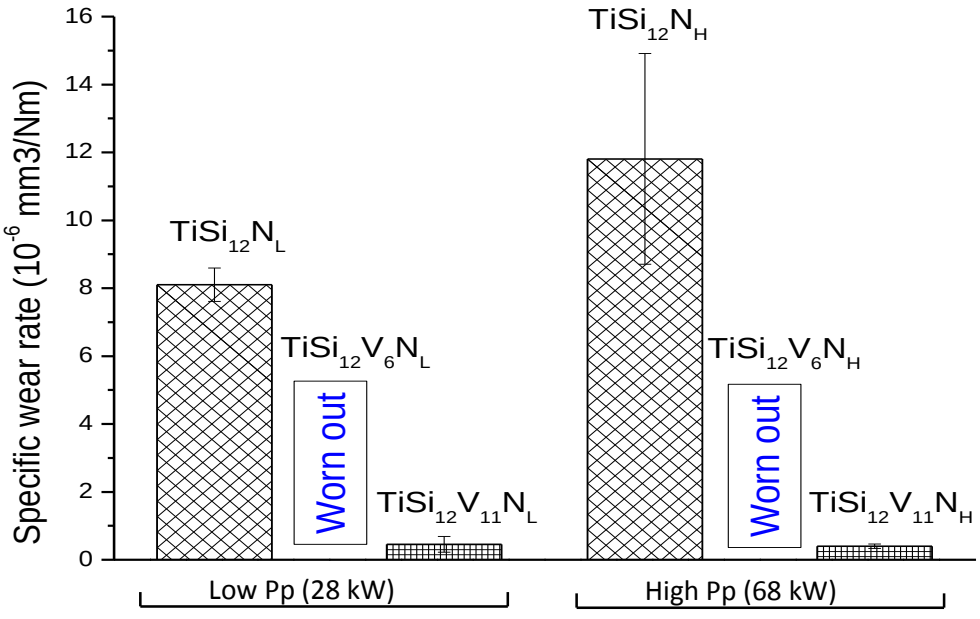

(b) 12 at.% Si

Figure 5.9. Wear rate of the dissimilar coatings. (a) TiSi(V)N coatings with 7 at.% Si, (b) TiSi(V)N coatings with 12 at.% Si.

Figure 5.10 displays the typical 2D wear track profiles of the coatings. As explained above, the wear tracks of $TiSi_{12}V_6N_1$ and $TiSi_{12}V_6N_2$ displayed the highest wear depth (3 and 2 µm, respectively) with complete worn out of the films caused by the low adhesion of these films to the substrate as the critical scratch load values revealed. Further, it can also be seen that coatings with 11 at.% vanadium content (figure 5.10 a, b) showed the shallowest wear tracks so that

almost no signs of wear were seen in the profile measurements indicating the excellent wear resistance of these coatings.

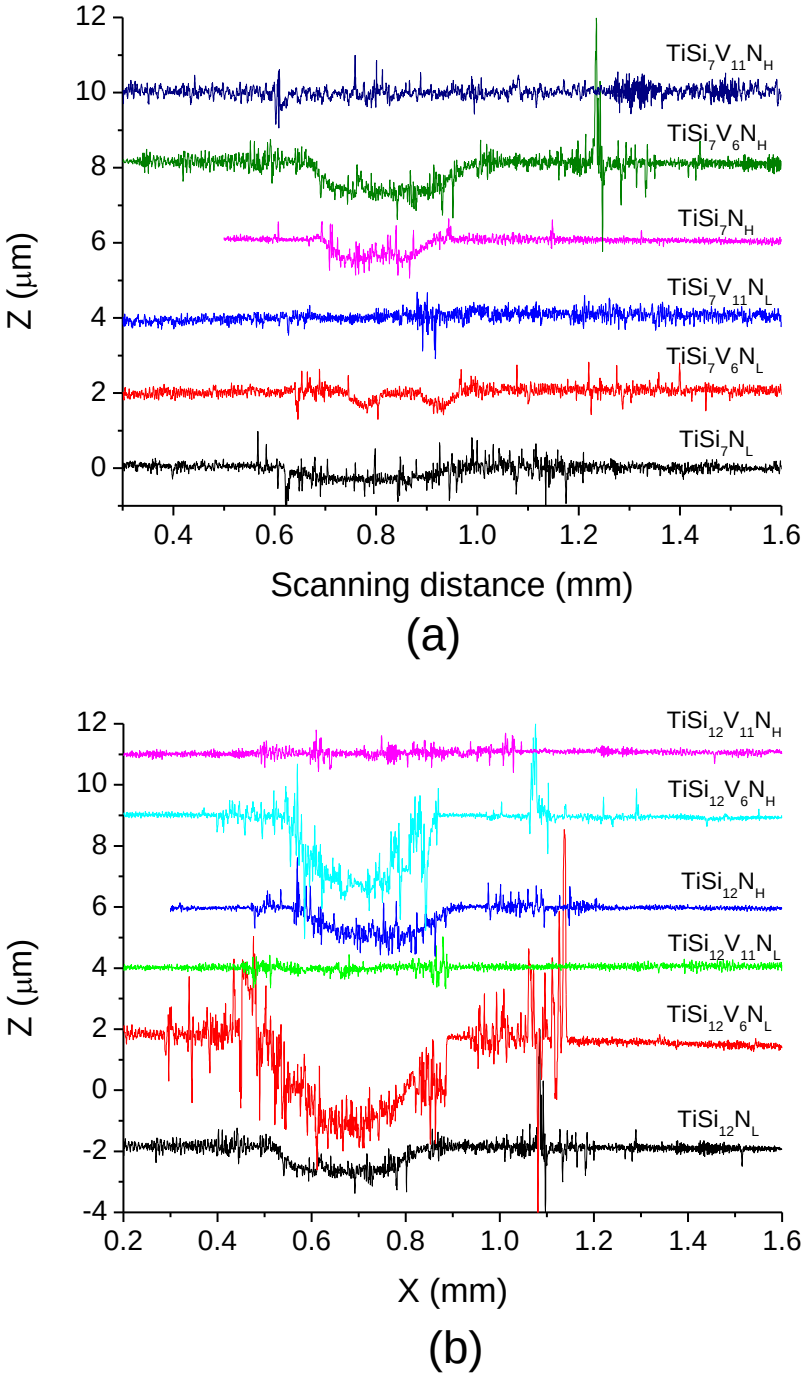

Figure 5.10. 2D wear track profiles of dissimilar TiSi(V)N coatings. (a) with 7 at.% Si, and (b). with 12 at.% Si

5.6.2. Friction Coefficient

Reciprocating sliding test friction curves of the films tested at room temperature are shown in figure 5.11. All friction curves exhibited running-in stage where friction coefficient increased with increasing in number of cycles resulted from the contact stress variations and the rough surface, and steady state stages with relatively smooth curve and constant friction coefficient values. In all the cases, additions of vanadium reduced the friction coefficient (COF) of TiSiN

coatings. However, some differences on COF were observed depending on the Si content on films and on the peak powers used. For coatings deposited with 7 at.% Si at low peak power (figure 5.11, a), a successive reduction of the friction coefficient was noticed with V additions, in good agreement with the decrease of wear rate (see figure 5.9). For the same series of films deposited with high peak power (figure 5.11, a), a decrease of friction coefficient was also noticed with increasing V content. However, such decrease was of lower magnitude as compared to the coatings deposited with low peak power. Further, the friction coefficient of these coatings showed to be independent of the V content on the films. Coatings deposited with 12 at.% Si (figure 5.11, c – d) displayed higher COF than those deposited with 7 at.% of Si. However, a higher decrease of friction coefficient was observed for coatings deposited with low peak power (figure 5.11, c).

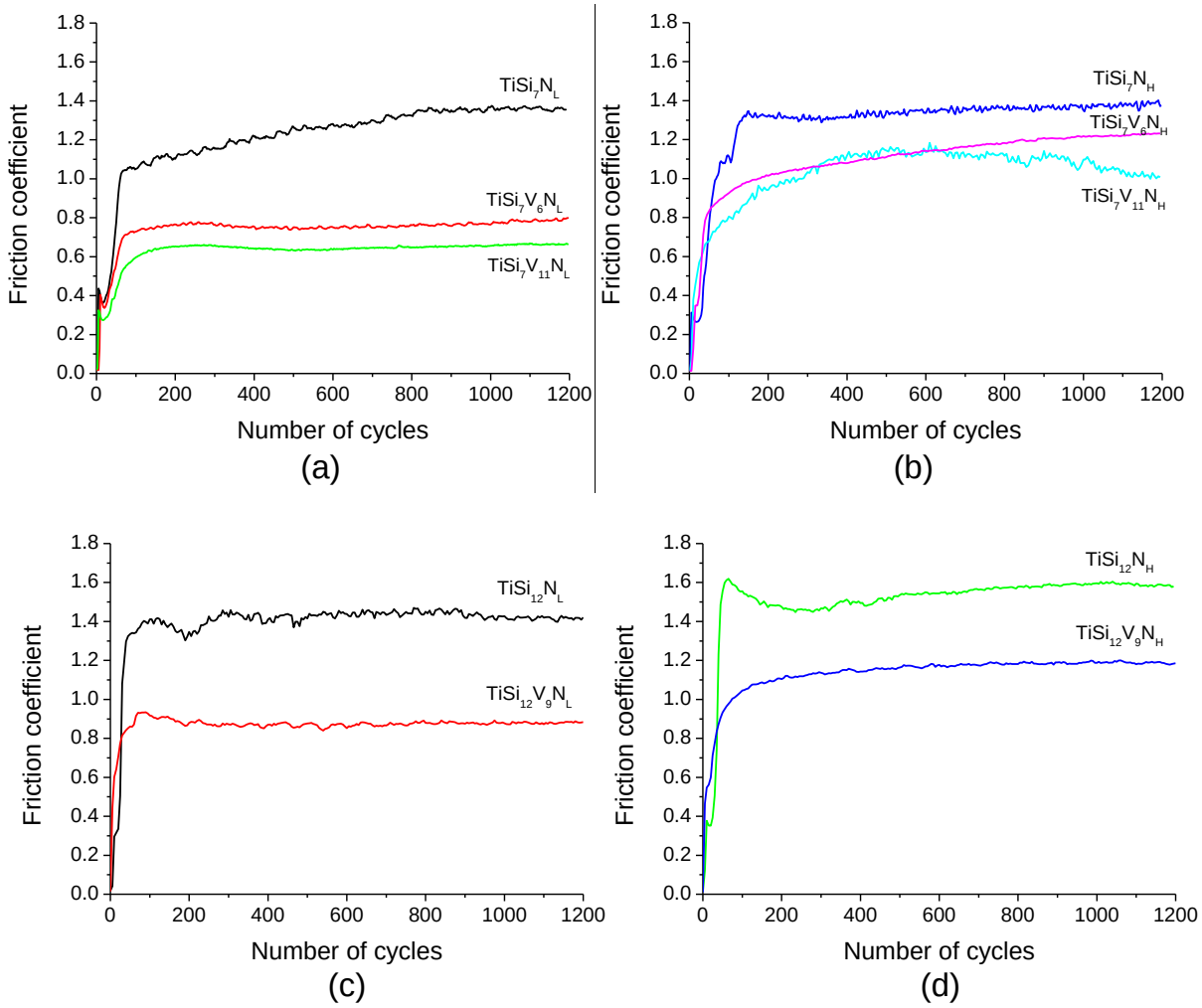

Figure 5.11. Friction coefficient vs number of cycles of dissimilar TiSi(V)N films for reciprocating sliding test at room temperature. (a) TiSi(V)N with 7 at.% Si deposited at low Pp, (b) TiSi(V)N with 7 at.% Si deposited at high Pp, (c) TiSi(V)N with 12 at.% Si deposited at low Pp, (d) TiSi(V)N with 12 at.% Si deposited at high Pp.

5.6.3. Wear mechanisms

Since the changes in the friction coefficient and wear rates described above are only partially correlated with the applied test conditions and structural and/or mechanical properties of the films, scanning electron microscopy (SEM) analysis was conducted on the worn surfaces of coatings in order to identify the main wear mechanisms produced. In addition, EDS and Raman

analysis were also carried out in order to identify the composition of wear debris present on the worn surface of coatings and balls.

5.6.3.1. Coatings containing 7 at.% Si

TiSiN coating deposited with high peak power showed better wear resistance than those deposited with low peak power (figure 5.9, a). Abrasive wear was the main active wear mechanism present in both cases as revealed by the abrasion grooves parallel to the relative sliding movement observed on the wear track of the coatings (figure 5.12 a, b). Thus, such increase of wear resistance could only be explained based on the increase of hardness and improvement of compactness of films as referred before. Needle shaped wear debris particles were observed inside of the wear tracks of coatings. Further, some of these particles were seen tied in on the end of some grooves indicating that they are the responsible for the abrasive wear. EDS analysis performed at these wear debris particles (appendix C, figure C1) showed that they are mainly composed of oxygen, titanium, silicon, and traces of aluminium suggesting the presence of Ti-O, Si-O, and transferred material from the counter body (Al_2O_3). For low peak power, V additions progressively decreased the wear rates and friction coefficient of coatings (figure 5.9 a, figure 5.11 a). SEM images of the wear track revealed mild abrasive (polishing) wear as the main wear mechanism. The wear track becomes shallower and smoother with the increase in V content in the coatings. Figure 5.12 c) displays the typical wear track of TiSiVN coating deposited at low peak power with 6 at.% V. Hardness cannot be the cause for the improved wear resistance of these coatings, as the hardness values for these coatings are equivalent or lower than for reference TiSiN coating. EDS analysis carried out on the wear debris observed on the worn surface of this coating indicated that they are composed of O, Ti, V, Si, and traces of Al (appendix C, figure C2 - C3) suggesting the presence of T-O, V-O, Si-O and Al-O oxides. Raman analysis performed at the same wear debris confirmed the presence of Rutile (TiO_2) and V_2O_5 (see figure 5.13). Thus, the progressive improvement of wear resistance and reduced friction with V additions could be attributed to the presence of lubricious V_2O_5.

TiSiVN coatings deposited at high peak powers exhibited polishing wear similar to those deposited using low peak power. V addition for these coatings initially showed an increase in wear rate and then a very low wear rate with further increase in V content (figure 5.9, a). Although V addition reduced friction coefficient, the decrease in friction coefficient with vanadium addition was lower as compared to those deposited at low peak power (figure 5.11 a, b). The higher wear rate for TiSiVN coating with 6 at.% V can be ascribed to the low cohesive strength (figure 5.8 e), table 5.4). The $TiSi_7V_{11}N_H$ coating with 11 at.% V, with 7 at.% Si deposited at high Pp showed the best wear resistance of all the coatings. This behaviour can be attributed to the combined effect of presence of lubricious V_2O_5, high level of compactness of the microstructure, and high hardness as compared to the coatings produced with low peak power.

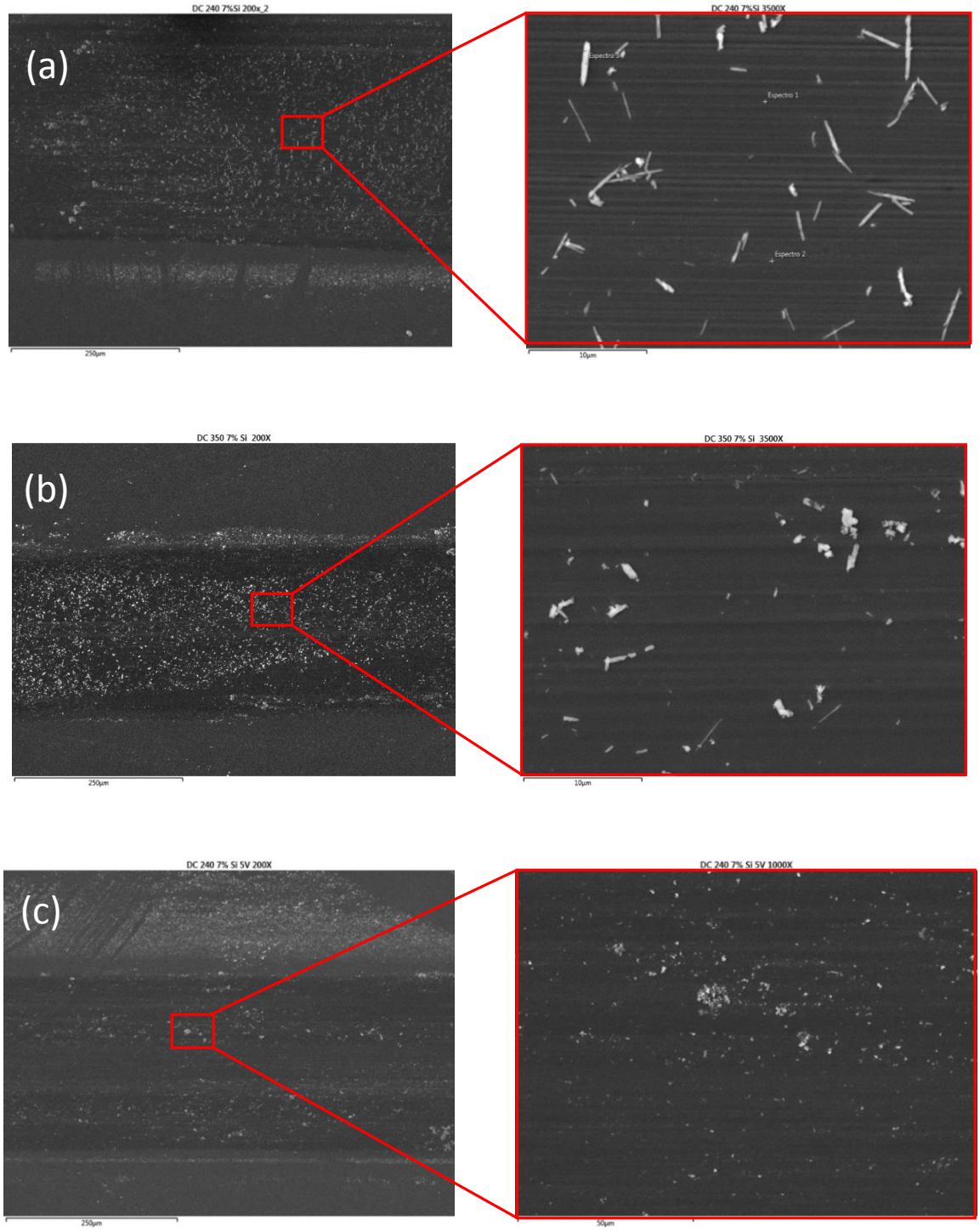

Figure 5.12. SEM wear track images of dissimilar TiSi(V)N coatings with 7 at.% of Si deposited at low and high peak power. (a) $TiSi_7N_L$ and (b) $TiSi_7N_H$, (c) $TiSi_7V_6N_L$

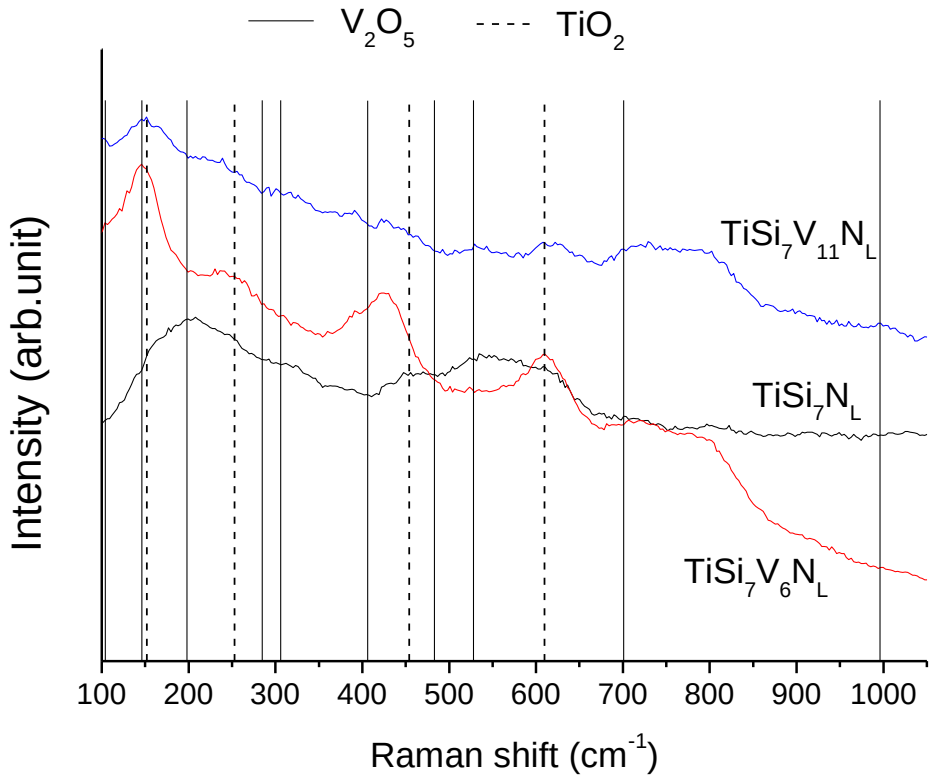

Figure 5.13. Typical Raman spectra obtained from wear debris particles of dissimilar TiSi(V)N films

5.6.3.2. Coatings containing 12 at.% Si

Both TiSiN coatings deposited at low and high peak powers showed abrasive wear mechanism similar to TiSiN coatings deposited with 7at.% Si. In general, TiSiN coatings with 12 at.% Si showed higher wear rates than those with 7 at.% Si. This agrees well with the literature [60], and can be attributed to the formation of the amorphous Si_3N_4 in the films. TiSiN deposited at high peak power ($TiSi_{12}N_H$) showed higher wear rate as compared to the one deposited at low peak power ($TiSi_{12}N_L$). This is imputed to the brittle behaviour of this coating, as suggested by the cracks detected on its wear track (figure 5.14). A complete delamination of the TiSiN coatings was observed with the first increase of V content. This behaviour showed to be independent of the peak power, and can be ascribed to the low adhesion critical load values of these coatings (figure 5.8 h) and k)). Further increase of V additions, decreased the wear rate of the reference TiSiN films. As for V rich coatings deposited with 7 at.% Si, this behaviour showed to be related to the presence of lubricious V_2O_5 phase on the wear track of these coatings. Polishing wear mechanism was also observed for these coatings (films containing 12 at.% Si with V additions). EDS results performed on the worn out surfaces of coatings with 12 at.% Si can be found in Appendix C (figures C4 – C5).

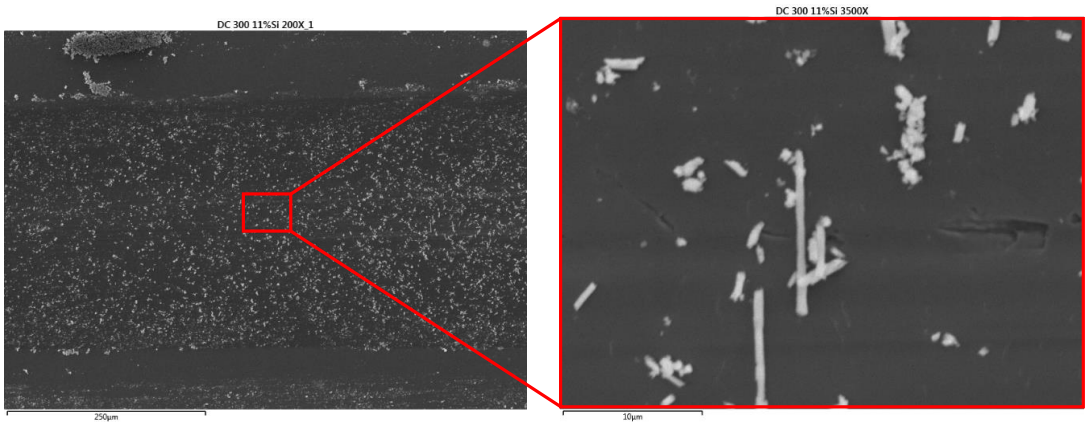

Figure 5.14. SEM wear track images of TiSiVN coatings with 12 at.% of Si deposited at low and high peak power ($TiSi_{12}N_H$).

As a summary, all films with highest vanadium content (11 at.% V), irrespective of silicon amount and peak power used, showed the best tribological behaviour among all the coatings. This behaviour could be attributed to the formation of vanadium oxide which protects the coatings from wear.

Conclusions

In this thesis, the effect of V addition on the structure, mechanical properties and tribological behaviour of Ti-Si-V-N films deposited by HiPIMS in DOMS mode was studied. SEM images of the coatings revealed that increasing the peak power provided dense coatings. Si content and V addition didn't show any significant change on the cross section and surface morphology of the coatings. XRD patterns of all coatings showed an fcc-type structure assigned to crystalline TiN. A shift of diffraction peaks to higher angles with addition of V indicated the formation of substitutional solid solution within the TiN lattice. Hardness and Young's modulus of the coatings with V additions did not show any regular evolution. However, coatings deposited at high peak power showed higher hardness and higher level of compressive residual stresses as compared to those deposited at low peak powers.

Tribological test results showed that alloying TiSiN with V decreases both friction coefficient and wear rate of coatings. TiSiVN films with highest V content (11 at.% V) showed excellent wear resistance among all the coatings. SEM-EDS and Raman analysis revealed that this improvement in tribological properties is due to the formation of lubricious V-O phase on the contact zone. Abrasive wear was identified on the wear track of the dissimilar TiSiN films deposited as reference, while polishing wear was the main wear mechanism detected on the worn surface of the V rich films.

Future work

Oxidation tests will be carried out to study if the coating structures allow controlled release of vanadium to the surface, a condition necessary for long lasting lubrication. Since the potential industrial application area of these coatings is high temperature lubrication, tribological tests at high temperatures (500 – 700 ^{o}C) will be performed as well.

References

[1] C. Muratore, J. Hu, A. Voevodin, *Adaptive nanocomposite coatings with a titanium nitride diffusion barrier mask for high-temperature tribological applications,* Thin Solid Films. 515 (2007) 3638–3643.

[2] K. Kutschej, P. Mayrhofer, M. Kathrein, P. Polcik, C. Mitterer, *A new low-friction concept for Ti 1- x Al x N based coatings in high-temperature applications,* Surface and Coatings Technology. 188 (2004) 358–363.

[3] N. Fateh, G. Fontalvo, G. Gassner, C. Mitterer, *Influence of high-temperature oxide formation on the tribological behaviour of TiN and VN coatings,* Wear. 262 (2007) 1152–1158.

[4] K. Kutschej, P. Mayrhofer, M. Kathrein, P. Polcik, C. Mitterer, *Influence of oxide phase formation on the tribological behaviour of Ti-Al-V-N coatings,* Surface and Coatings Technology. 200 (2005) 1731–1737.

[5] F. Fernandes, A. Loureiro, T. Polcar, A. Cavaleiro, *The effect of increasing V content on the structure, mechanical properties and oxidation resistance of Ti-Si-V-N films deposited by DC reactive magnetron sputtering,* Applied Surface Science. 289 (2014) 114–123.

[6] E. Londero, E. Schröder, *Vanadium pentoxide (V 2 O 5): A van der Waals density functional study,* Computer Physics Communications. 182 (2011) 1805–1809.

[7] G. Gassner, P. Mayrhofer, K. Kutschej, C. Mitterer, M. Kathrein, *A new low friction concept for high temperatures: lubricious oxide formation on sputtered VN coatings,* Tribology Letters. 17 (2004) 751–756.

[8] Z. Zhou, W. Rainforth, D. Lewis, S. Creasy, J. Forsyth, F. Clegg, et al., *Oxidation behaviour of nanoscale TiAlN/VN multilayer coatings,* Surface and Coatings Technology. 177 (2004) 198–203.

[9] F.D. Fernandes, *Surface modification of molds and accessories for the glass industry,* Ph.D thesis, University of Coimbra, 2014.

[10] K. Jun, Y. Shimogaki, *Development of TiSiN CVD process using TiCl 4/SiH 4/NH 3 chemistry for ULSI anti-oxidation barrier applications,* Science and Technology of Advanced Materials. 5 (2004) 549–554.

[11] K.-D. Bouzakis, G. Skordaris, S. Gerardis, G. Katirtzoglou, S. Makrimallakis, M. Pappa, et al., *Ambient and elevated temperature properties of TiN, TiAlN and TiSiN PVD films and their impact on the cutting performance of coated carbide tools,* Surface and Coatings Technology. 204 (2009) 1061–1065.

[12] J. Oliveira, F. Fernandes, F. Ferreira, A. Cavaleiro, *Tailoring the nanostructure of Ti-Si-N thin films by HiPIMS in Deep Oscillations Magnetron Sputtering (DOMS) mode,* Surface and Coatings Technology. 264 (2015) 140 - 149.

[13] T. committee of petroleum additive manufacturers in Europe, *Lubricant additives and the environment*, ATC Document. 49 (2007).

[14] Organisation for economic co-operation, development, *Emmission scenario document on lubricants and lubricant additives*, OECD Environmental Health and Safety Publications: Series on Emission Scenario Documents. (2004).

[15] M. Pfeiler, K. Kutschej, M. Penoy, C. Michotte, C. Mitterer, M. Kathrein, *The effect of increasing V content on structure, mechanical and tribological properties of arc evaporated Ti-Al-V-N coatings*, International Journal of Refractory Metals and Hard Materials. 27 (2009) 502–506.

[16] G. Stachowiak, A.W. Batchelor, *Engineering tribology*, Butterworth-Heinemann, 2013.

[17] A. Voevodin, C. Muratore, S. Aouadi, *Hard coatings with high temperature adaptive lubrication and contact thermal management: review*, Surface and Coatings Technology. 257 (2014) 247–265.

[18] J. Zabinski, J. Sanders, J. Nainaparampil, S. Prasad, *Lubrication using a microstructurally engineered oxide: performance and mechanisms*, Tribology Letters. 8 (2000) 103–116.

[19] K turbo, *Airfoil bearings* [Online]. 2014 [Accessed 9 December 2014]. Available from: http://www.turboblower.net/part_1.pdf.

[20] S. Aouadi, H. Gao, A. Martini, T. Scharf, C. Muratore, *Lubricious oxide coatings for extreme temperature applications: A review*, Surface and Coatings Technology. 257 (2014) 266–277.

[21] A. Irving, J. Ibets, *High-Speed Bearing Technologies for Wastewater Treatment Applications*, Proceedings of the Water Environment Federation. 2013 (2013) 98–106.

[22] T. Scharf, S. Prasad, *Solid lubricants: a review*, Journal of Materials Science. 48 (2013) 511–531.

[23] S. Aouadi, B. Luster, P. Kohli, C. Muratore, A. Voevodin, *Progress in the development of adaptive nitride-based coatings for high temperature tribological applications*, Surface and Coatings Technology. 204 (2009) 962–968.

[24] A. Erdemir, *A crystal chemical approach to the formulation of self-lubricating nanocomposite coatings*, Surface and Coatings Technology. 200 (2005) 1792–1796.

[25] P.M. Martin, *Handbook of deposition technologies for films and coatings: science, applications and technology*, William Andrew, 2009.

[26] P. Mayrhofer, P.E. Hovsepian, C. Mitterer, W.-D. Münz, *Calorimetric evidence for frictional self-adaptation of TiAlN/VN superlattice coatings*, Surface and Coatings Technology. 177 (2004) 341–347.

[27] E. Lugscheider, O. Knotek, K. Bobzin, S. Bärwulf, *Tribological properties, phase generation and high temperature phase stability of tungsten-and vanadium-oxides*

deposited by reactive MSIP-PVD process for innovative lubrication applications, Surface and Coatings Technology. 133 (2000) 362–368.

[28] R. Franz, C. Mitterer, *Vanadium containing self-adaptive low-friction hard coatings for high-temperature applications: A review*, Surface and Coatings Technology. 228 (2013) 1–13.

[29] H. Wriedt, *The OV (oxygen-vanadium) system*, Bulletin of Alloy Phase Diagrams. 10 (1989) 271–277.

[30] ASM Handbook, *Alloy phase diagrams*, vol. 3. ASM International, 1992.

[31] S. Beke, *A review of the growth of V 2 O 5 films from 1885 to 2010,* Thin Solid Films. 519 (2011) 1761–1771.

[32] R. Franz, J. Schnöller, H. Hutter, C. Mitterer, *Oxidation and diffusion study on AlCrVN hard coatings using oxygen isotopes 16 O and 18 O*, Thin Solid Films. 519 (2011) 3974–3981.

[33] Y. Qiu, S. Zhang, J.-W. Lee, B. Li, Y. Wang, D. Zhao, *Self-lubricating CrAlN/VN multilayer coatings at room temperature,* Applied Surface Science. 279 (2013) 189–196.

[34] J.H. Ouyang, S. Sasaki, *Tribo-oxidation of cathodic arc ion-plated (V, Ti) N coatings sliding against a steel ball under both unlubricated and boundary-lubricated conditions,* Surface and Coatings Technology. 187 (2004) 343–357.

[35] M. Uchida, N. Nihira, A. Mitsuo, K. Toyoda, K. Kubota, T. Aizawa, *Friction and wear properties of CrAlN and CrVN films deposited by cathodic arc ion plating method,* Surface and Coatings Technology. 177 (2004) 627–630.

[36] Y. Qiu, S. Zhang, B. Li, Y. Wang, J.-W. Lee, F. Li, et al., *Improvement of tribological performance of CrN coating via multilayering with VN*, Surface and Coatings Technology. 231 (2013) 357–363.

[37] J.-K. Park, Y.-J. Baik, *Increase of hardness and oxidation resistance of VN coating by nanoscale multilayered structurization with AlN,* Materials Letters. 62 (2008) 2528–2530.

[38] K. Bobzin, N. Bagcivan, M. Ewering, R. Brugnara, S. Theiß, *DC-MSIP/HPPMS (Cr, Al, V) N and (Cr, Al, W) N thin films for high-temperature friction reduction,* Surface and Coatings Technology. 205 (2011) 2887–2892.

[39] F. Fernandes, J. Morgiel, T. Polcar, A. Cavaleiro, *Oxidation and diffusion processes during annealing of TiSi (V) N films,* Surface and Coatings Technology. 275 (2015) 120-126.

[40] F. Fernandes, T. Polcar, A. Cavaleiro, *Tribological properties of self-lubricating TiSiVN coatings at room temperature,* Surface and Coatings Technology. 267 (2014) 8-14.

[41] J. Lin, W.D. Sproul, J.J. Moore, Z. Wu, S. Lee, R. Chistyakov, et al., *Recent advances in modulated pulsed power magnetron sputtering for surface engineering,* JOM. 63 (2011)

48–58.

[42] D. Lundin, *The HiPIMS Process.* Ph.D. thesis, Linkoping University, 2010.

[43] F. Ferreira, R. Serra, J. Oliveira, A. Cavaleiro, *Effect of peak target power on the properties of Cr thin films sputtered by HiPIMS in deep oscillation magnetron sputtering (DOMS) mode,* Surface and Coatings Technology. 258 (2014) 249–256.

[44] D. Camino, D. Teer, J. Von Stebut, M. Gee, N. Jennett, J. Banks, et al., *Scratch adhesion testing of coated surfaces-Challenges and new directions, Adhesion Measurement of Films \& Coatings:* Volume 2. 2 (2001) 79.

[45] D. Christie, *Fundamentals of high power pulsed magnetron sputtering: Visualization of mechanisms for rate reduction and increased ion fraction,* Czechoslovak Journal of Physics. 56 (2006) B93–B97.

[46] R. Behrisch, W. Eckstein, *Sputtering by particle bombardment: experiments and computer calculations from threshold to MeV energies,* Springer Science \& Business Media, 2007.

[47] F. Vaz, L. Rebouta, S. Ramos, M. da Silva, J. Soares, *Physical, structural and mechanical characterization of Ti 1- x Si x N y films,* Surface and Coatings Technology. 108 (1998) 236–240.

[48] F. Vaz, L. Rebouta, B. Almeida, P. Goudeau, J. Pacaud, J. Riviere, et al., *Structural analysis of Ti 1- x Si x N y nanocomposite films prepared by reactive magnetron sputtering,* Surface and Coatings Technology. 120 (1999) 166–172.

[49] V. Chawla, R. Jayaganthan, R. Chandra, *A study of structural and mechanical properties of sputter deposited nanocomposite Ti-Si-N thin films,* Surface and Coatings Technology. 204 (2010) 1582–1589.

[50] M.A.P. Yazdi, F. Lomello, J. Wang, F. Sanchette, Z. Dong, T. White, et al., *Properties of TiSiN coatings deposited by hybrid HiPIMS and pulsed-DC magnetron co-sputtering,* Vacuum. 109 (2014) 43–51.

[51] H. Windischmann, *Intrinsic stress in sputter-deposited thin films,* Critical Reviews in Solid State and Material Sciences. 17 (1992) 547–596.

[52] A. Niederhofer, T. Bolom, P. Nesladek, K. Moto, C. Eggs, D. Patil, et al., *The role of percolation threshold for the control of the hardness and thermal stability of super-and ultrahard nanocomposites,* Surface and Coatings Technology. 146 (2001) 183–188.

[53] M. Hála, J. \vCapek, O. Zabeida, J. Klemberg-Sapieha, L. Martinu, *Pulse management in high power pulsed magnetron sputtering of niobium,* Surface and Coatings Technology. 206 (2012) 4186–4193.

[54] M. Pfeiler, K. Kutschej, M. Penoy, C. Michotte, C. Mitterer, M. Kathrein, *The influence of bias voltage on structure and mechanical/tribological properties of arc evaporated Ti-Al-V-N coatings,* Surface and Coatings Technology. 202 (2007) 1050–1054.

[55] K. Kutschej, P. Mayrhofer, M. Kathrein, P. Polcik, R. Tessadri, C. Mitterer, *Structure, mechanical and tribological properties of sputtered Ti 1-x Al x N coatings with 0.5≤ x≤ 0.75*, Surface and Coatings Technology. 200 (2005) 2358–2365.

[56] S. Veprek, M.G. Veprek-Heijman, P. Karvankova, J. Prochazka, *Different approaches to superhard coatings and nanocomposites*, Thin Solid Films. 476 (2005) 1–29.

[57] S. Vep\vrek, S. Reiprich, *A concept for the design of novel superhard coatings*, Thin Solid Films. 268 (1995) 64–71.

[58] I. Camps, S. Muhl, E. Camps, J. Quiñones-Galván, M. Flores, *Tribological properties of TiSiN thin films deposited by laser ablation*, Surface and Coatings Technology. 255 (2014) 74–78.

[59] J. Patscheider, T. Zehnder, M. Diserens, *Structure-performance relations in nanocomposite coatings*, Surface and Coatings Technology. 146 (2001) 201–208.

[60] J. Xu, H. Ju, L. Yu, *Influence of silicon content on the microstructure, mechanical and tribological properties of magnetron sputtered Ti-Mo-Si-N films*, Vacuum. 110 (2014) 47–53.

[61] Y. Cheng, T. Browne, B. Heckerman, E. Meletis, *Mechanical and tribological properties of nanocomposite TiSiN coatings*, Surface and Coatings Technology. 204 (2010) 2123–2129.

[62] J. Lin, J.J. Moore, W.D. Sproul, B. Mishra, Z. Wu, J. Wang, T*he structure and properties of chromium nitride coatings deposited using dc, pulsed dc and modulated pulse power magnetron sputtering*, Surface and Coatings Technology. 204 (2010) 2230–2239.

Annex A

F. Fernandes, M.A. Mekicha, J.C. Oliveira, T. Polcar, A. Cavaleiro. *Lubricious TiSi(V)N coatings for extreme temperature application deposited by Deep Oscillation Magnetron Sputtering (DOMS) mode.* Ibertrib 2015. Proceedings of the VIII Iberian Conference on Tribology: Conference Proceedings. Cartagena: Universidad Politécnica de Cartagena, Servicio de Documentación, 2015. Pp.287 – 294, ISBN: 978-84-606-8904-1.

Lubricious TiSi(V)N coatings for extreme temperature application deposited by Deep Oscillation Magnetron Sputtering (DOMS) mode

F. Fernandes[1*], M.A. Mekicha[1], J.C. Oliverira[1], T. Polcar[2, 3], A. Cavaleiro[1]
[1]SEG-CEMUC - Department of Mechanical Engineering, University of Coimbra, Rua Luís Reis Santos, 3030-788 Coimbra, Portugal.
[2]National Centre for Advanced Tribology (nCATS), School of Engineering Sciences, University of Southampton, Highfield, Southampton, SO17 1BJ, UK.
[3]Department of Control Engineering Czech Technical University in Prague Technicka 2, Prague 6, 166 27 Czech Republic.
*e-mail: filipe.fernandes@dem.uc.pt

ABSTRACT

Development of new self-lubricant coating systems with control of the lubricous species diffusion have enormous potential to be used in the protection of surfaces in components for machining. In the last years, vanadium rich coatings have been introduced as possible candidates for self-lubrication due to their optimum tribological properties. This work is devoted on the study of V additions on the morphology, structure and on the tribological properties of TiSiN films deposited by HiPIMS in Deep Oscillation Magnetron Sputtering (DOMS) mode. Two different peak powers were used on the deposition of coatings in order to produce films with different morphology. The tribological properties of coatings were evaluated at room temperature against Al_2O_3 balls on a pin-on-disc apparatus. Increasing of peak power showed to change the cross section morphology of films from columnar type to compact structure. V additions improved the tribological properties of TiSiN coatings.

KEY WORDS: Lubricious TiSi(V)N films, DOMS, Tribology

1. INTRODUCTION

Dictated by elimination of coolant media utilisation and environmental protection requirements, recently milling and cutting operations are making a transition to dry machining. This shift in machining technology requires machining tools to withstand harsh working conditions combining oxidation, abrasion, adhesion, thermal and mechanical loads. Solid lubricant coatings such as diamond like carbons (DLCs), transition metal dichalcogenides (TMD), and WC/C have been used in improving performance and lifetime of the cutting tools. However, their tribological properties degrade in humid atmospheres and/or at elevated temperatures due to their low oxidation resistance. To overcome this shortcoming, a new concept of high temperature lubrication has been proposed. Solid lubricant coatings have been developed by combining the intrinsic properties of some binary or ternary films (TiN, CrN, CrAlN, TiAlN, YSZ, etc), which are very hard and resistant to oxidation, with specific elements (metals), which diffuse to the surface and form a low friction tribolayer (as a metal layer, e.g. Ag, Cu, Au, Pb and In, or a low-friction oxide, e.g. V_2O_5, $Ag_2Mo_2O_7$) [1-4]. Among these elements, particular attention has been given to the vanadium-containing coatings (Magnéli phases V_nO_{2n-1}), which showed interesting tribological properties in the temperature range 500–700 ºC [5-11].

Dissimilar series of V-based hard coatings have been developed, such as ternary CrVN [12], (V,Ti)N [13], multilayer AlN/VN [14] and quaternary single layered or multilayered AlCrVN [15, 16] and TiAlVN [8, 17-19]. Independently of the configuration, the friction was decreased and the wear resistance improved. However, such improvements were of short duration due to the rapid release of vanadium. The quick out diffusion of V from the coating results in the consequent loss of the low friction

properties after few minutes [20]. The control of V out-diffusion is now one of the major challenges to achieve a suitable long lasting wear and friction properties without compromising the original properties of the host binary and ternary films. Therefore, one possible proposal to solve this problem is to use coating systems with a dual phase structure, such as the case of TiSiN system, in which one of the phases (Si_3N_4) could act as a diffusion barrier to the lubricious phase metal (V) release.

The purpose of this work is to study the effect of V addition on high temperature tribological properties of TiSi(V)N coatings deposited by high power impulse magnetron sputtering (HiPIMS) in deep oscillation mode (DOMS) as it has been reported to allow easily tailor the nanocomposite structure of the TiSiN films; condition necessary to produce films with proper barrier to the lubricious species to achieve long term lubrication [21]. TiSiN system was selected because of its very high oxidation resistance similar to TiAlN, and TiCrN but can be deposited with much better mechanical properties. Two series of coatings (using two different peak powers) were deposited with increasing V content, in order to evaluate the effect of V addition on the surface and cross section morphology, structure and tribological properties of TiSiN films.

2. EXPERIMENTAL PROCEDURE

Six TiSi(V)N films were deposited in reactive, unbalanced mode by DOMS (HiPIMS Cyprium™III plasma generator, Zpulser Inc.) at a deposition pressure of 1.2 Pa without bias. Prior to the depositions, all the substrates were ultrasonically cleaned in acetone and alcohol. The substrates were then mounted in a rotating (18 revs/min) substrate holder. A square (150 × 150 mm) of high purity Ti (99.9%) target with 20 holes (10 mm in diameter) uniformly distributed throughout the preferential erosion zone was used. The holes were filled with different number of pellets of high purity Si (99.9%) and high purity V (99.9%), in order to achieve a desired Si and V content, with the remaining holes filled with Ti pellets. A total of six depositions were made. All the coatings were deposited with 7% of Si using two different peak powers (28.31 kW and 109.83 kW), with increasing V content (0, 5, and 10 at.%, achieved by using 0, 5, and 9 pellets of V at the Ti target, respectively). Hereinafter the coatings will be designated as $TiSiN_y$, or $TiSiV_xN_y$ where y denotes the peak power and x the number of V pellets introduced at the Ti target. Thus, coatings with y = 1 and 2 means that the coatings were deposited with peak powers of 29.31 kW and 109.83 kW, respectively. Table 1 shows the sample designation adopted for coatings identification. Before making the deposition, the chamber was evacuated down to 5×10^{-4} Pa. Ion gun plasma was used to clean the substrates before depositions. The films were deposited onto silicon wafers for structure analysis, cross section, surface morphology characterization and chemical composition evaluation; stainless steel discs (Ø 20 × 1 mm) for residual stress measurements and AISI M2 (Ø 24 x 7.9 mm) substrates for tribological characterization. The chemical composition of the coatings was evaluated by energy dispersive spectroscopy (EDS). TiSiN and TiSiVN films with different Si and V contents as measured by Electron Probe Microanalysis (EPMA), from previous depositions [22], were used as reference for the EDS measurements. The chemical composition of the films are plotted in Table 2. Scanning electron microscopy (SEM) was used to examine the thickness, fracture cross section and surface morphologies of films. The crystallographic structure was investigated by X-ray diffraction (X' Pert Pro MPD diffractometer) using a grazing incidence angle of 3º and Cu Kα1 radiation (λ = 1.54060 A). The tribological behavior of films was evaluated on a pin-on-disc tribometer at room temperature, using 5N normal load, 5.3 mm wear track radius, 10 cm/s linear speed

and 3000 cycles. Al_2O_3 ball of grade 20 with diameter 7.94 mm was used as a counterpart. The friction coefficient was continuously measured and the wear rate of films determined from the wear track using a Zygo – NewView 7200, 3D profilometer.

Table 1 - Sample designation of coatings.

Coating	Number of V pellets	Peak power (kW)	Designation
TiSiN	0	28.31	$TiSiN_1$
TiSiVN	5		$TiSiV_5N_1$
	9		$TiSiV_9N_1$
TiSiN	0	109.83	$TiSiN_2$
TiSiVN	5		$TiSiV_5N_2$
	9		$TiSiV_9N_2$

Table 2 - Chemical composition of the coatings in at.%.

Coating	at.%			
	N	Si	V	Ti
$TiSiN_1$	52.0 ± 0.5	7.1 ± 0.1	40.9 ± 0.5	
$TiSiV_5N_1$	50.7 ± 0.5	7.1 ± 0.2	35.7 ± 0.5	6.4 ± 0.3
$TiSiV_9N_1$	50.2 ± 0.5	6.8 ± 0.1	31.0 ± 0.4	12.0 ± 0.3
$TiSiN_2$	52.0 ± 0.3	6.8 ± 0.1	41.2 ± 0.3	
$TiSiV_5N_2$	51.2 ± 0.1	7.1 ± 0.1	36.0 ± 0.5	5.8 ± 0.3
$TiSiV_9N_2$	50.6 ± 0.4	6.8 ± 0.1	30.5 ± 0.1	12.1 ± 0.5

3. RESULTS AND DISCUSSION

3.1. Surface and cross section morphology of coatings

Figure 1 displays the effect of change of peak power and increasing V content on the surface and fracture cross section micrographs of TiSi(V)N coatings. Coatings deposited with the low peak power (Figures 1 a), b) and c)) showed a typical columnar structure, while, the ones deposited with the high peak power (Figs. 1 d), e) and f)) displayed a compact morphology, although some very small remains columns are still observed. The increasing of compactness level can be attributed to the increasing of the bombarding species energy with increasing peak power [21]. As V content was increased, in both TiSiN reference films, the columns size and the surface roughness were increased.

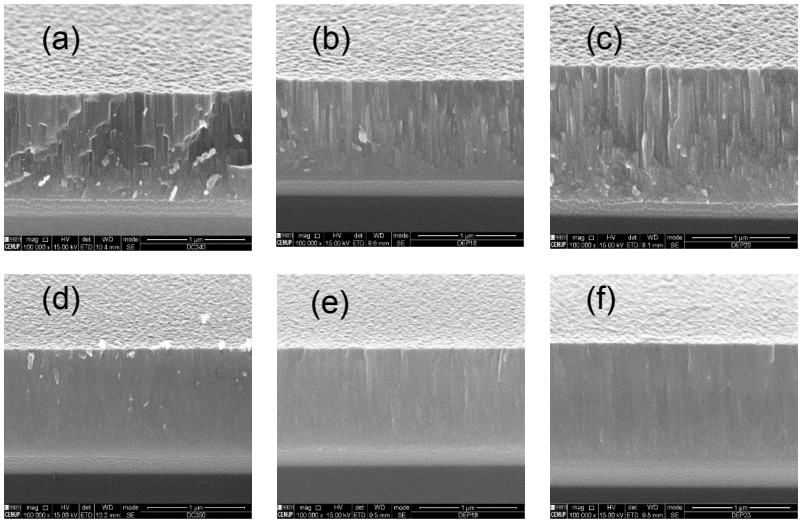

Figure 1 - Surface and cross section morphology of coatings deposited with low peak and high peak power. Low peak power: (a), (b), (c) $TiSiN_1$, $TiSiV_5N_1$, $TiSiV_9N_1$ respectively; and high peak power: (d), (e), (f) $TiSiN_2$, $TiSiV_5N_2$, $TiSiV_9N_2$, respectively.

3.2. Structure

The corresponding X-ray diffraction patterns of the as-deposited coatings are displayed in figure 2. The effect of the peak power on the structure of the coatings is shown in spectrums a) and b), whilst the effect of V additions in each of the previous TiSiN films is displayed in spectrums c-d and e-f for coatings deposited with low and high peak power, respectively. All the diffraction peaks could be generally assigned to the f.c.c NaCl type TiN phase. However, depending on the power supply used and on the V content on the films, different peak positions, intensities and broadening can be observed. Increasing the peak power on TiSiN films shift the diffraction peaks to lower angles. Such behavior can be attributed to the increase of compressive residual stresses on the film with increasing peak power. Compressive residual stresses of 1.96 and 2.99 GPa were calculated (based on the Stoney equation) for the TiSiN films deposited with low and high peak power, respectively. The increase of the level of compressive residual stresses with increasing peak power can be attributed to the increase of ions energy, as reported elsewhere [21]. With increasing V content, the fcc peaks are shifted to higher angles, behavior associated to a smaller unit cell. Since similar levels of compressive residual stresses were measure for each series of the V rich coatings in respect to the references TiSiN films, this behavior can only be explained by substitution of Ti by the smaller V atoms, which due to its smaller atomic radius promotes the contraction of the TiN lattice. Similar trend was observed by Pfeiler et al. [17] for the TiAlVN system and by Fernandes et al. [22] for TiSi(V)N system deposited by DC reactive magnetron sputtering.

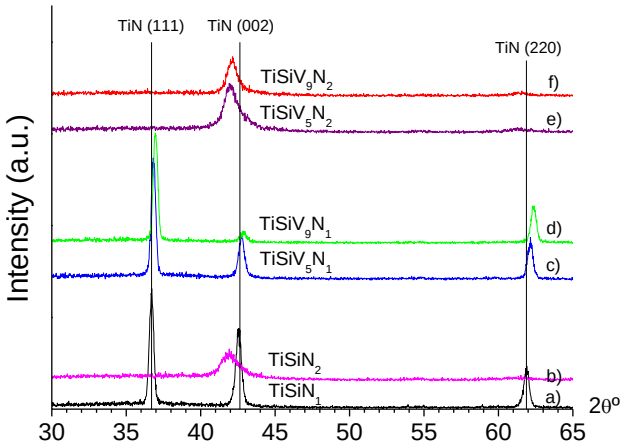

Figure 2 - X–ray diffraction patterns of TiSi(V)N films deposited with increasing peak power and with increasing V content. a) $TiSiN_1$, b) $TiSiN_2$, c) $TiSiV_5N_1$, d) $TiSiV_9N_1$, e) $TiSiV_5N_2$, f) $TiSiV_9N_2$.

3.3. Tribological behavior

Figure 3 shows the friction coefficient, specific wear rate and the 2D profiles of the wear track of the different coatings tested against Al_2O_3. TiSiN coating deposited with low peak power showed higher specific wear rate than coating produced with high peak power. This result agrees with the friction coefficient values and can be attributed to the high hardness of the $TiSiN_2$ film (31.55 against 22.9 GPa for $TiSiN_1$ film). In all cases, the addition of vanadium resulted in a reduction of the friction coefficient (see figure 3 (a)) and also on the improvement of the wear resistance. These improvements in tribological properties can be attributed to the formation of lubricious vanadium oxides on the wear track of coatings as revealed EDS and Raman analysis (not shown here).

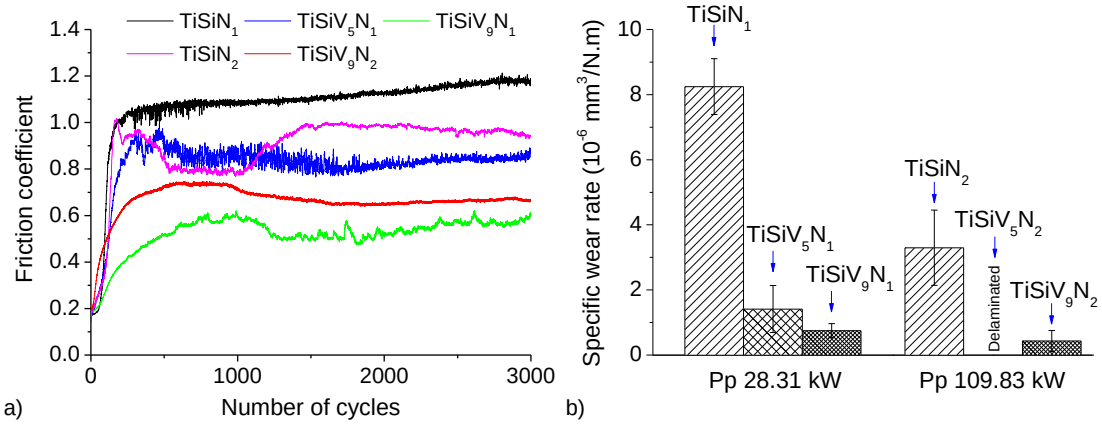

Figure 3 - (a) friction coefficient, (b) specific wear rate, and (c) 2D wear track profile of TiSi(V)N coatings.

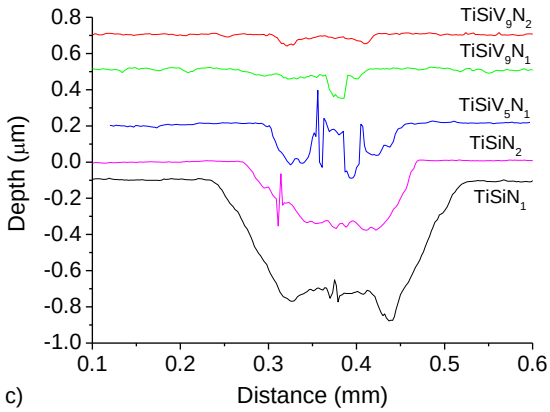

Figure 3 (continued)

4. CONCLUSION

The results showed that independently of the peak power used on the deposition and/or the v content present on the films, all the coatings displayed diffraction peaks assigned to crystalline f.c.c NaCl type TiN phase. The increase of peak power in TiSiN films showed to shift the diffraction peaks to lower angles, behavior attributed to the increasing of the bombarding species energy with increasing peak power, which increases the level of compressive residual stresses on the films. A shift of the diffraction peaks to higher angles is observed with increasing V content on the TiSiN films, suggesting the formation of a substitutional solid solution in TiN phase. This behavior showed to be independent of the peak power applied on the coatings although different changes in peaks intensity and broadening were noticed. V additions to TiSiN films decreased the wear rate and the friction coefficient of coatings, due to vanadium oxide formation.

ACKNOWLEDGEMENTS

This research is sponsored by FEDER funds through the program COMPETE – Programa Operacional Factores de Competitividade – and by national funds through FCT – Fundação para a Ciência e a Tecnologia, under the projects: PTDC/EME-TME/122116/2010 and PTDC/EMS-TEC/1805/2012. The authors acknowledge the Master student Melkamu A. Mekicha (co-author of this paper) from the International Joint European Master in Tribology of Surfaces and Interfaces (TRIBOS) program, doing his thesis in the mechanical engineering department of the University of Coimbra, for his special dedication on the development of this research.

REFERENCES

[1] S.M. Aouadi, H. Gao, A. Martini, T.W. Scharf, C. Muratore, Lubricious oxide coatings for extreme temperature applications: A review, Surf. Coat. Technol. 257 (2014) 266-277.
[2] R. Franz, C. Mitterer, Vanadium containing self-adaptive low-friction hard coatings for high-temperature applications: A review, Surf. Coat. Technol., 228 (2013) 1-13.
[3] T.W. Scharf, S.V. Prasad, Solid lubricants: a review, J. Mater. Sci., 48 (2013) 511-531.
[4] A.A. Voevodin, C. Muratore, S.M. Aouadi, Hard coatings with high temperature adaptive lubrication and contact thermal management: review, Surf. Coat. Technol. 257 (2014) 247-265.

[5] N. Fateh, G.A. Fontalvo, G. Gassner, C. Mitterer, Influence of high-temperature oxide formation on the tribological behavior of TiN and VN coatings, Wear, 262 (2007) 1152-1158.
[6] D.B. Lewis, S. Creasey, Z. Zhou, J.J. Forsyth, A.P. Ehiasarian, P.E. Hovsepian, Q. Luo, W.M. Rainforth, W.D. Münz, The effect of (Ti+Al):V ratio on the structure and oxidation behavior of TiAlN/VN nano-scale multilayer coatings, Surf. Coat. Technol., 177–178 (2004) 252-259.
[7] K. Kutschej, P.H. Mayrhofer, M. Kathrein, P. Polcik, C. Mitterer, A new low-friction concept for Ti1−xAlxN based coatings in high-temperature applications, Surf. Coat. Technol., 188–189 (2004) 358-363.
[8] K. Kutschej, P.H. Mayrhofer, M. Kathrein, P. Polcik, C. Mitterer, Influence of oxide phase formation on the tribological behavior of Ti–Al–V–N coatings, Surf. Coat. Technol., 200 (2005) 1731-1737.
[9] G. Gassner, P.H. Mayrhofer, K. Kutschej, C. Mitterer, M. Kathrein, A New Low Friction Concept for High Temperatures: Lubricious Oxide Formation on Sputtered VN Coatings, Tribology Letters, 17 (2004) 751-756.
[10] P.H. Mayrhofer, P.E. Hovsepian, C. Mitterer, W.D. Münz, Calorimetric evidence for frictional self-adaptation of TiAlN/VN superlattice coatings, Surf. Coat. Technol., 177–178 (2004) 341-347.
[11] A. Glaser, S. Surnev, F.P. Netzer, N. Fateh, G.A. Fontalvo, C. Mitterer, Oxidation of vanadium nitride and titanium nitride coatings, Surface Science, 601 (2007) 1153-1159.
[12] M. Uchida, N. Nihira, A. Mitsuo, K. Toyoda, K. Kubota, T. Aizawa, Friction and wear properties of CrAlN and CrVN films deposited by cathodic arc ion plating method, Surf. Coat. Technol., 177–178 (2004) 627-630.
[13] J.H. Ouyang, S. Sasaki, Tribo-oxidation of cathodic arc ion-plated (V,Ti)N coatings sliding against a steel ball under both unlubricated and boundary-lubricated conditions, Surf. Coat. Technol., 187 (2004) 343-357.
[14] J.-K. Park, Y.-J. Baik, Increase of hardness and oxidation resistance of VN coating by nanoscale multilayered structurization with AlN, Mater. Lett., 62 (2008) 2528-2530.
[15] R. Franz, J. Neidhardt, R. Kaindl, B. Sartory, R. Tessadri, M. Lechthaler, P. Polcik, C. Mitterer, Influence of phase transition on the tribological performance of arc-evaporated AlCrVN hard coatings, Surf. Coat. Technol., 203 (2009) 1101-1105.
[16] Y. Qiu, S. Zhang, J.-W. Lee, B. Li, Y. Wang, D. Zhao, Self-lubricating CrAlN/VN multilayer coatings at room temperature, Applied Surface Science, 279 (2013) 189-196.
[17] M. Pfeiler, K. Kutschej, M. Penoy, C. Michotte, C. Mitterer, M. Kathrein, The effect of increasing V content on structure, mechanical and tribological properties of arc evaporated Ti–Al–V–N coatings, International Journal of Refractory Metals and Hard Materials, 27 (2009) 502-506.
[18] W. Tillmann, S. Momeni, F. Hoffmann, A study of mechanical and tribological properties of self-lubricating TiAlVN coatings at elevated temperatures, Tribology International, 66 (2013) 324-329.
[19] Q. Luo, Temperature dependent friction and wear of magnetron sputtered coating TiAlN/VN, Wear, 271 (2011) 2058-2066.
[20] F. Fernandes, PhD Thesis: Surface Modification of Molds and Acessories for the Glass Industry, Developed at the Mechanical Engineering Department of the University of Coimbra, University of Coimbra, Coimbra, 2014, Portugal.
[21] J.C. Oliveira, F. Fernandes, F. Ferreira, A. Cavaleiro, Tailoring the nanostructure of Ti–Si–N thin films by HiPIMS in deep oscillation magnetron sputtering (DOMS) mode, Surf. Coat. Technol., 264 (2015) 140-149.

[22] F. Fernandes, A. Loureiro, T. Polcar, A. Cavaleiro, The effect of increasing V content on the structure, mechanical properties and oxidation resistance of Ti–Si–V–N films deposited by DC reactive magnetron sputtering, Applied Surface Science, 289 (2014) 114-123.

Appendix A - TiN reference XRD pattern

Reference pattern: 1. TIN – REF. CODE: 01 – 087 – 0633

Name and formula

Reference code:	01-087-0633
Mineral name:	Osbornite, syn
ICSD name:	Titanium Azide
Empirical formula:	NTi
Chemical formula:	TiN

Crystallographic parameters

Crystal system:	Cubic
Space group:	Fm-3m
Space group number:	225
a (Å):	4.2380
b (Å):	4.2380
c (Å):	4.2380
Alpha (°):	90.0000
Beta (°):	90.0000
Gamma (°):	90.0000
Calculated density (g/cm^3):	5.40
Volume of cell (10^6 pm^3):	76.12
Z:	4.00
RIR:	4.06

Subfiles and Quality

Subfiles:	Inorganic, Mineral, Alloy, metal or intermetallic, Corrosion, Modelled additional pattern
Quality:	Calculated (C)

Comments

Sample preparation:	Sample prepared at 1172 for 2 days.
ICSD collection code:	064909
Test from ICSD:	No R value given. At least one TF missing.

References

Primary reference:	*Calculated from ICSD using POWD-12++*, (1997)
Structure:	Schoenberg, N., *Acta Chem. Scand.*, **8**, 213, (1954)

Peak list

No.	h	k	l	d [A]	2Theta[deg]	I [%]
1	1	1	1	2.44681	36.700	72.9
2	2	0	0	2.11900	42.633	100.0
3	2	2	0	1.49836	61.874	44.8
4	3	1	1	1.27781	74.145	17.3
5	2	2	2	1.22341	78.046	11.4

Stick Pattern

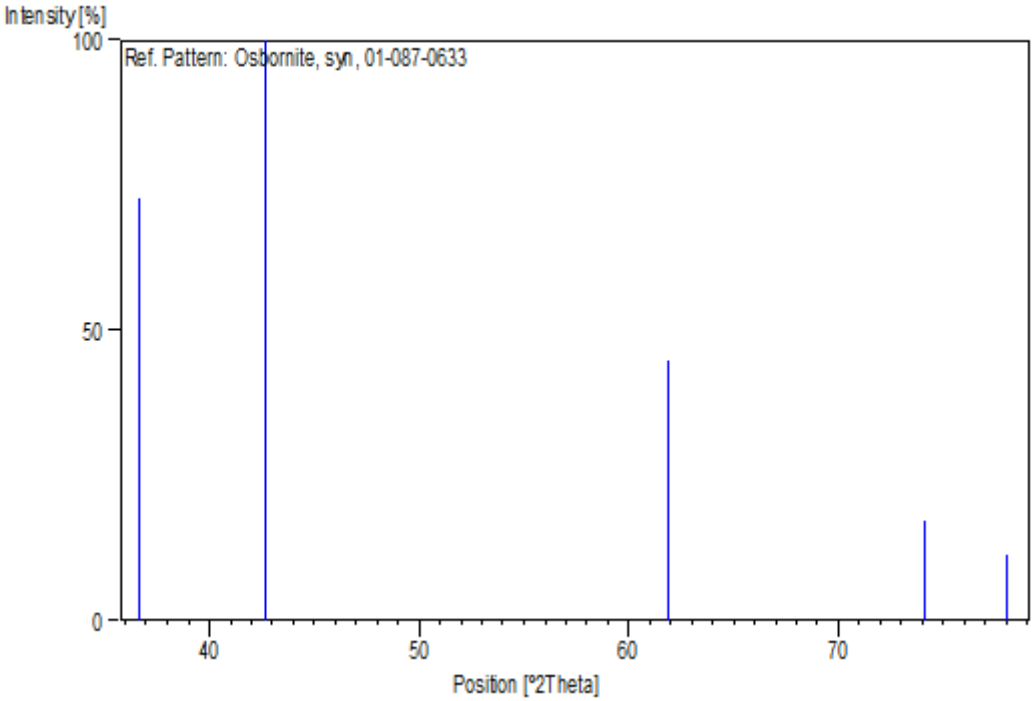

Appendix B - XRD patterns of dissimilar TiSi(V)N coatings obtained in grazing mode

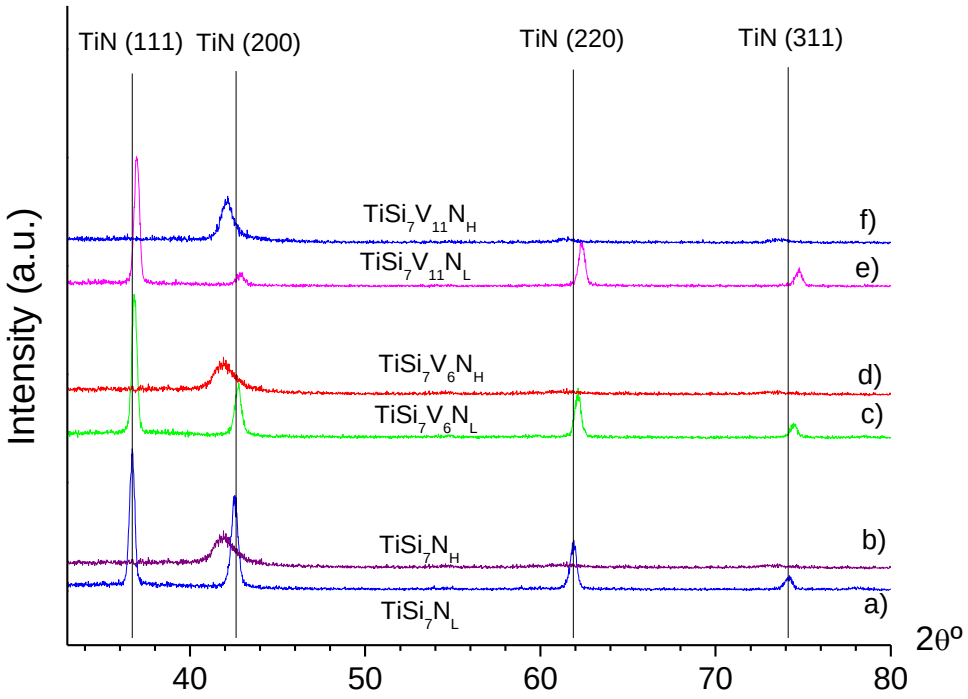

Figure B1. XRD pattern of TiSi(V)N films deposited with 7 at.% Si

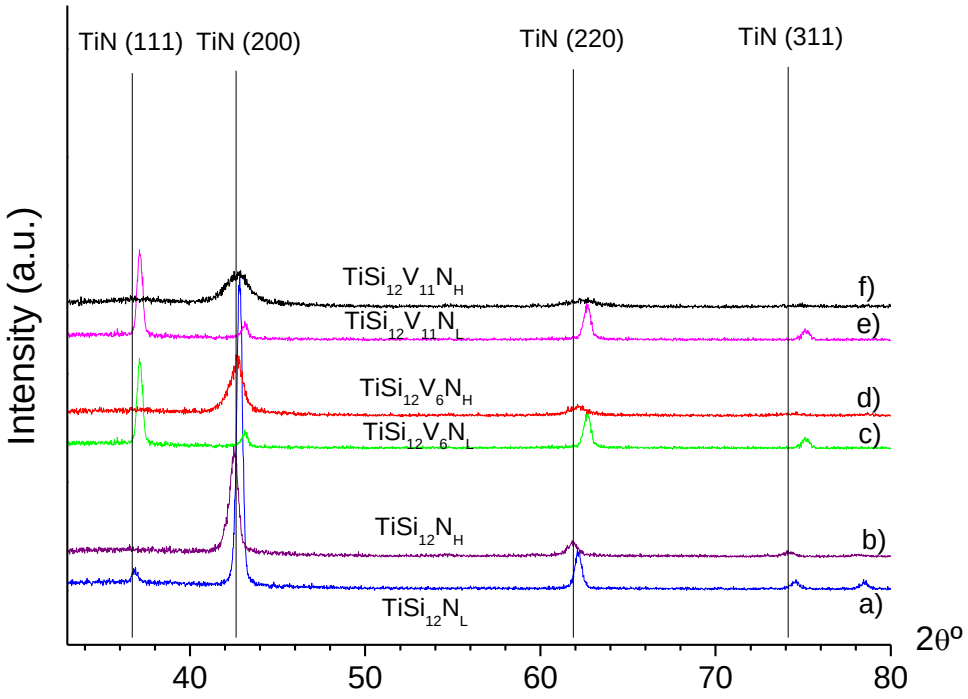

Figure B2. XRD pattern of TiSi(V)N films deposited with 12 at.% Si

Appendix C - SEM – EDS spectra of dissimilar coatings obtained on the wear debris

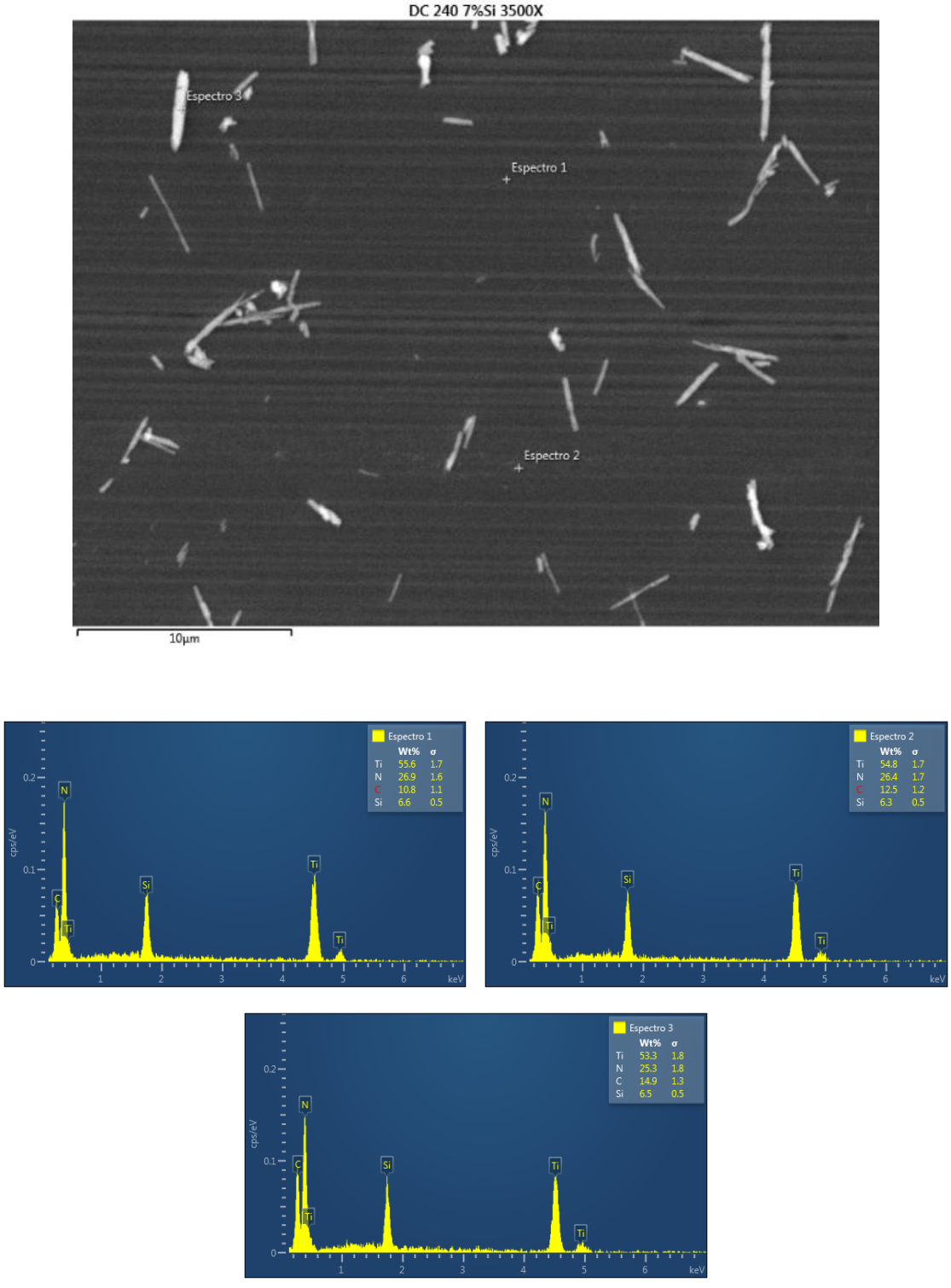

Figure C1. SEM - EDS spectra of $TiSi_7N_L$

***N.B.* spectro** – means spectrum

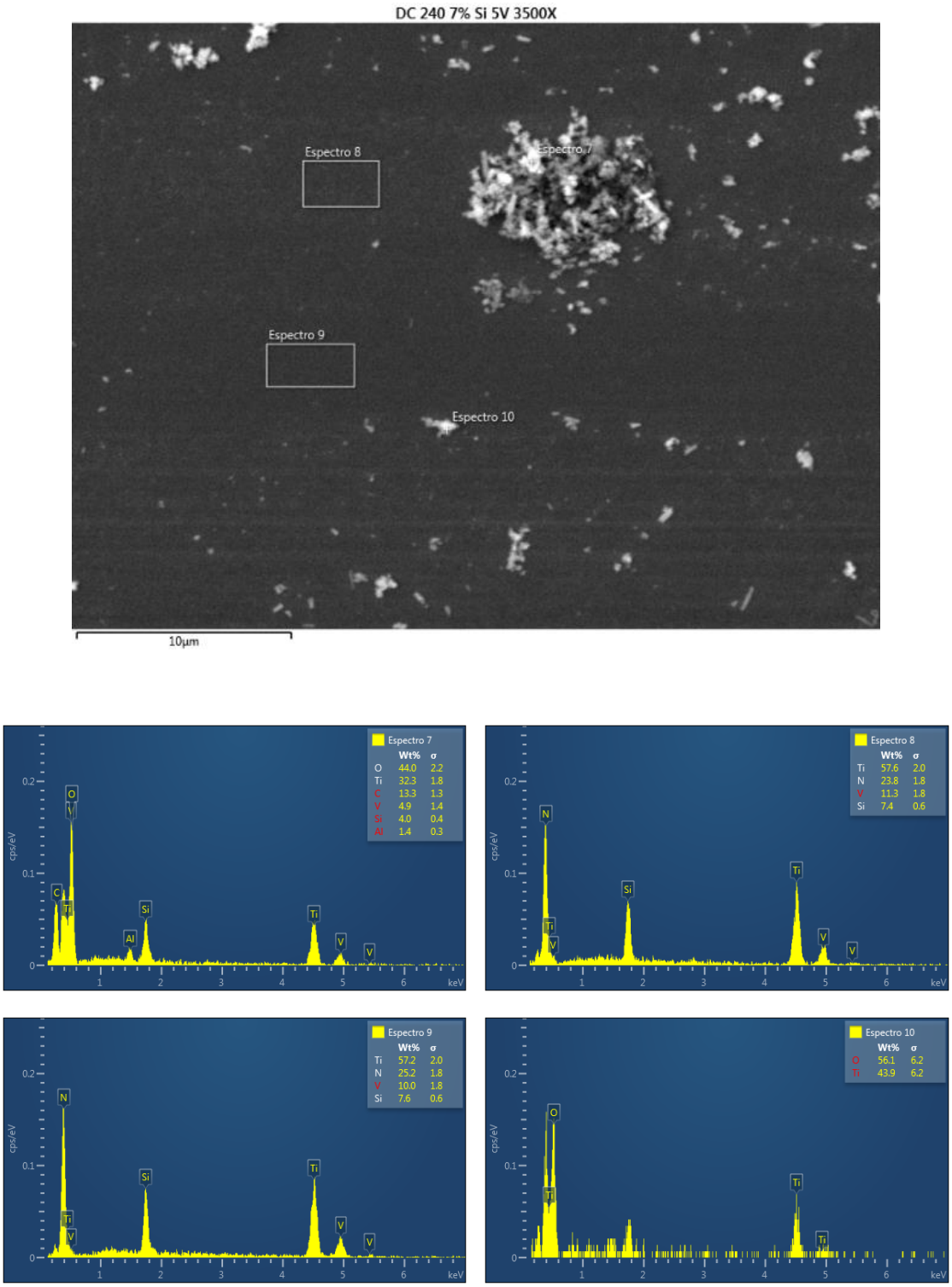

Figure C2. SEM - EDS spectra of $TiSi_7V_6N_L$

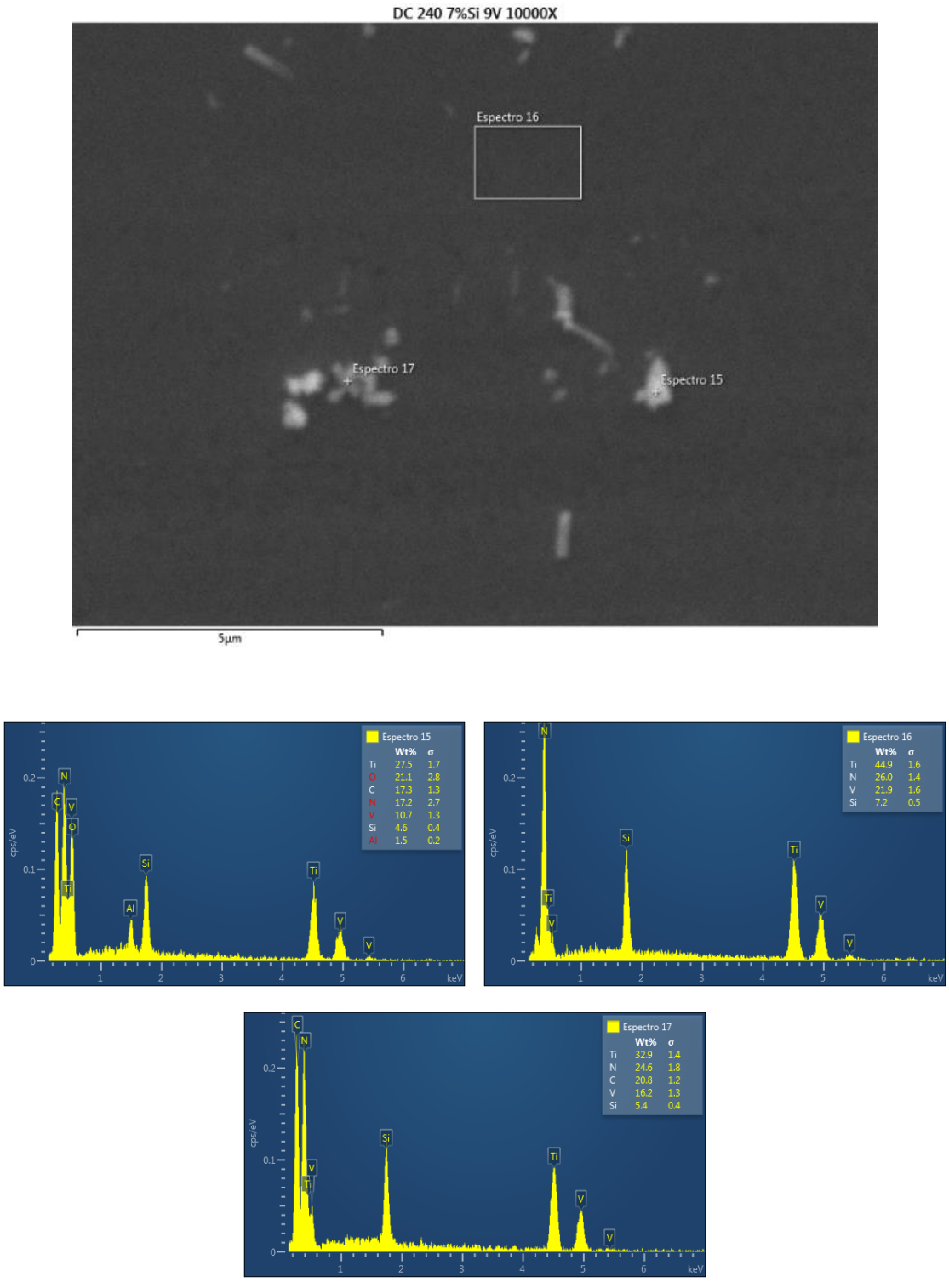

Figure C3. SEM - EDS spectra of $TiSi_7V_{11}N_H$

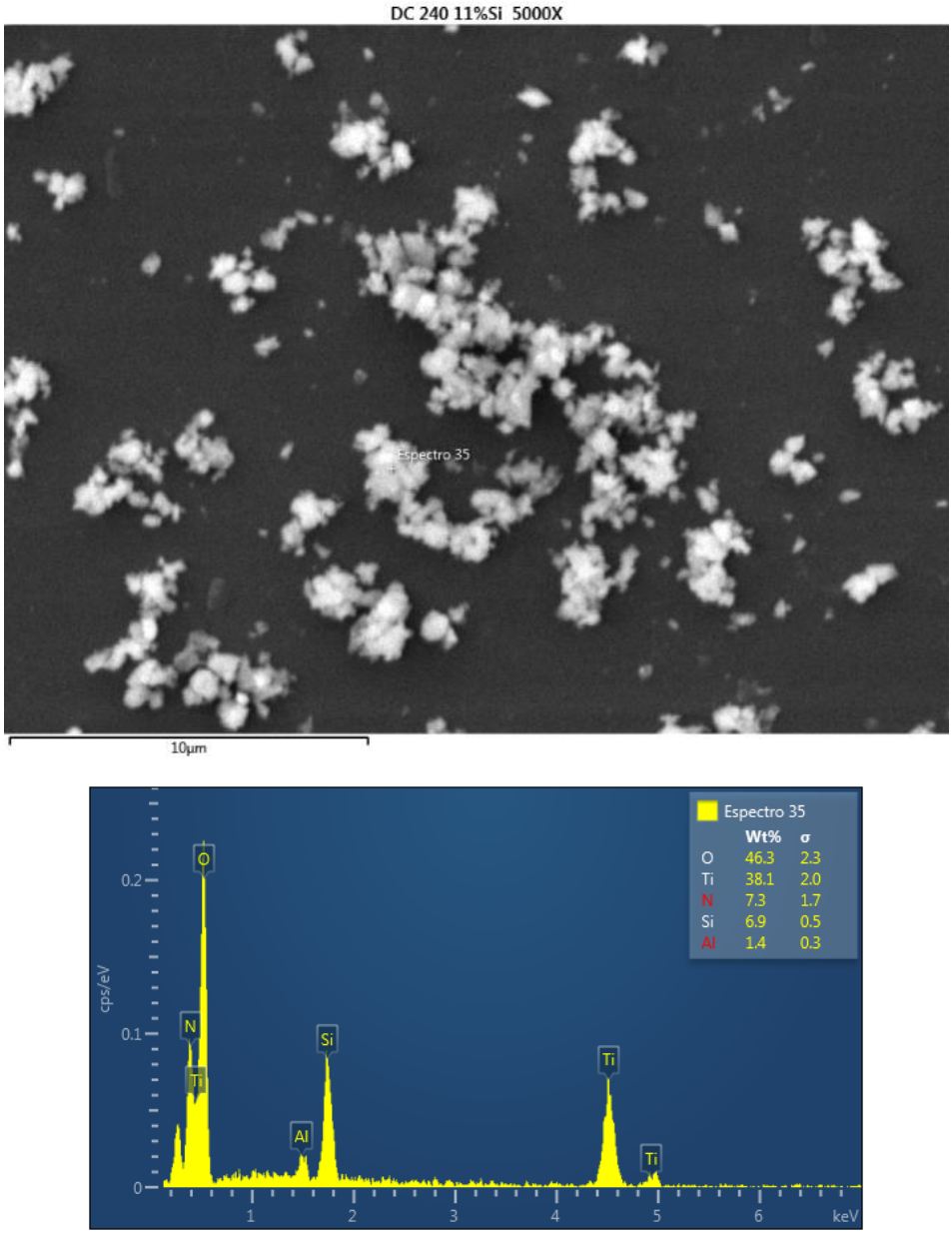

Figure C4. SEM - EDS spectra of $TiSi_{12}N_L$

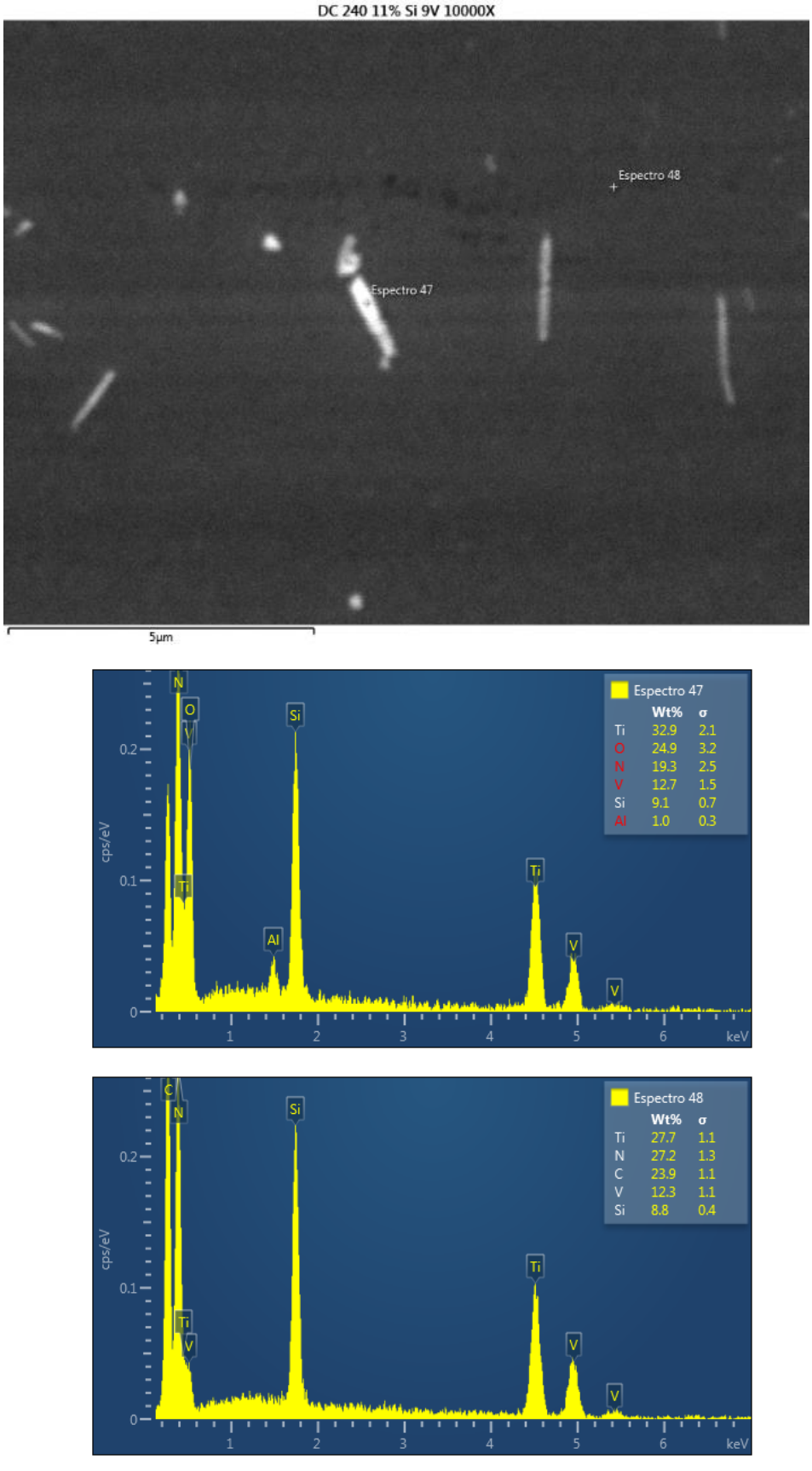

Figure C5. SEM - EDS spectra of $TiSi_{12}V_{11}N_L$